Polar Geosci., **16**, 196–226, 2003

Geochemistry and preliminary Sr-Nd isotopic data on the Neoproterozoic granitoids from the Bantoum area, west Cameroon: evidence for a derivation from a Paleoproterozoic to Archean crust

Charles Nzolang[1], Hiroo Kagami[1], Jean Paul Nzenti[2] and François Holtz[3]

[1] *Graduate School of Science and Technology, Niigata University, Ikarashi 2-nocho, Niigata 950-2181 (nzolang@gs.niigata-u.ac.jp)*
[2] *Département des Sciences de la Terre, Université de Yaoundé I, B.P. 812, Yaoundé, Cameroon*
[3] *Institut für Mineralogie, Universität Hannover, Callinstraβe 3, D-30167 Hannover, Germany*

(Received February 3, 2003; Accepted April 4, 2003)

Abstract: The Bantoum area in west Cameroon is composed of migmatitic gneisses associated with parallel strips of amphibolites, quartz-monzonites, biotite-granites, two-mica leucogranites and granitic dikes. Quartz-monzonites are metaluminous (A/CNK＝0.8–0.9) I-type, biotite-granites are peraluminous (A/CNK＝1.0–1.10) I-type, leucogranites are peraluminous (A/CNK＝1.14) S-type granitoids. All are hyper-potassic rocks defining a calc-alkaline trend. Quartz-monzonites gave an Rb-Sr isochron age of 720±61 Ma assumed to be a mixing age. The thermometry estimated from major elements and zircon saturation indicate that the biotite-granites crystallized from high temperature melts (812–866℃) whereas leucogranites crystallized from low temperature melts (719–745℃). The trace element distribution diagrams are characterized by an enrichment in LILE and LREE ($5 < La_N/Sm_N < 17$), with negative Nb, Ta, Sr and Ti anomalies. Model initial $^{87}Sr/^{86}Sr$ ratios (620 Ma) are 0.707614–0.708363 for quartz-monzonites, 0.711242–0.713784 for biotite-granites, and 0.715835 for leucogranites. They have highly negative ε_{Nd} (620 Ma) (-19~-11) and T_{DM} model ages ranging from 1.9 to 2.9 Ga. These geochemical and isotopic features imply that the granites are generated at different temperatures and from different crustal materials; they are the witnesses of the recycling of a Paleoproterozoic to Archean crust with minor inputs of juvenile magmas during the Pan-African orogeny. Chemical similarities between gneisses and some biotite-granites suggest that the partial melting of these gneisses may have contributed to the formation of granites.

key words: granite, geochemistry, Sr-Nd isotope, crustal recycling, west-Cameroon

1. Introduction

Since geochronological (Rb-Sr) works from Lasserre (1966, 1967), the Precambrian basement rocks in Cameroon was separated into the Archean Ntem complex (northwestern edge of Congo craton) in the south and the remaining territory belonging to the Pan-African "mobile zone"; the latter is now referred to as Central African fold belt (CAFB) (Penaye *et al*., 1993; Toteu *et al*., 2001) or Pan-African north-equatorial fold belt (Nzenti, 1987). The Ntem complex is essentially composed of charnockitic gneisses and various granitoids. Ages reported from recent works on that complex

range from 2.3 Ga for syenites (Pb-Pb zircon; Tchameni *et al*., 2001), 2.6 Ga for K-rich granitoids (Pb-Pb zircon; Tchameni *et al*., 2000) to 2.9 Ga for charnockites (U-Pb zircon; Toteu *et al*., 1994b). The CAFB in its Cameroon part (Fig. 1) is dominated by 500–700 Ma formations. It used to be roughly divided into 3 main lithotectonic units namely; (a) Paleoproterozoic basement predominantly composed of heterogeneous migmatitic gneisses; the study area is a part of this unit, (b) Meso- to Neoproterozoic volcano-sedimentary basins that are deformed and metamorphosed into schists and high-grade gneisses, and (c) Pan-African granitoids whose emplacement ages range from the early stage of the deformation (orthogneisses) to the late uplift stages of the belt (post-tectonic subcircular massifs), and that cross-cut the latter two units (Nzenti *et al*., 1988; Penaye *et al*., 1989; Toteu *et al*., 2001). However, using only petrological criteria, it is still difficult to distinguish between Neoproterozoic and Paleoproterozoic ages among high-grade rocks as remnants of Paleoproterozoic formations are common all over the fold belt.

Within the Precambrian basement in Cameroon, granitic rocks constitute the major component of the Pan-African terrains (Fig. 1) but they are still poorly known. Based on the compilation works from Bessoles and Trompette (1980), these granitic rocks are classified into two types, namely: the "circumscribed granites" that form wide massifs with well-delimited boundaries distinguishing them from their country rocks; they are mainly intrusive and show a homogeneity in texture and composition, and "not circumscribed granites" usually concordant with country rocks, the transition between the latter and granites being difficult to decipher; they show great variation in texture and structure and frequently contain enclaves. Bessoles and Trompette (1980) assumed that circumscribed granites are probably the more evolved terms of not circumscribed granites.

Some recent investigations have been carried out on some major magmatic complexes in west Cameroon: Ngondo granitic complex (Tagné Kamga, 1994; Tagné Kamga *et al*., 1999), Bangangté syenites (Tchouankoué, 1992), Batié granites (Talla, 1995), Fomopéa granites (Kwékam, 1993), Bandja charnockitic massif (Nguiessi Tchankam *et al*., 1997). All are interpreted by the above authors to be metaluminous, calc-alkaline and hyperpotassic syntectonic plutons, formed from mantle-derived magmas with little crustal contamination. Their emplacement ages (Rb-Sr whole rock) vary from 575 to 657 Ma; an U-Pb (zircon) age of 640±15 Ma is obtained on the Bandja charnockites (Nguiessi Tchankam and Vialette, 1994). But little is known concerning the so-called heterogeneous gneisses that are really associated with important exposures of granitoids as we will describe below in the Bantoum area in west Cameroon.

The sole work including this study area is reconnaissance survey of Weecksteen (1957) in which formations of the study area are simply mapped as hornblende-biotite gneisses. We believe that more detailed studies should be carried out on these heterogeneous migmatitic unit for a better understanding of their petrogenesis and the possibly link between gneisses and associated granitoids. In this paper we present the geochemistry and preliminary Rb-Sr and Sm-Nd isotopic data on granitoids and migmatitic gneisses from the Bantoum area, and discuss the nature of source materials of these rocks.

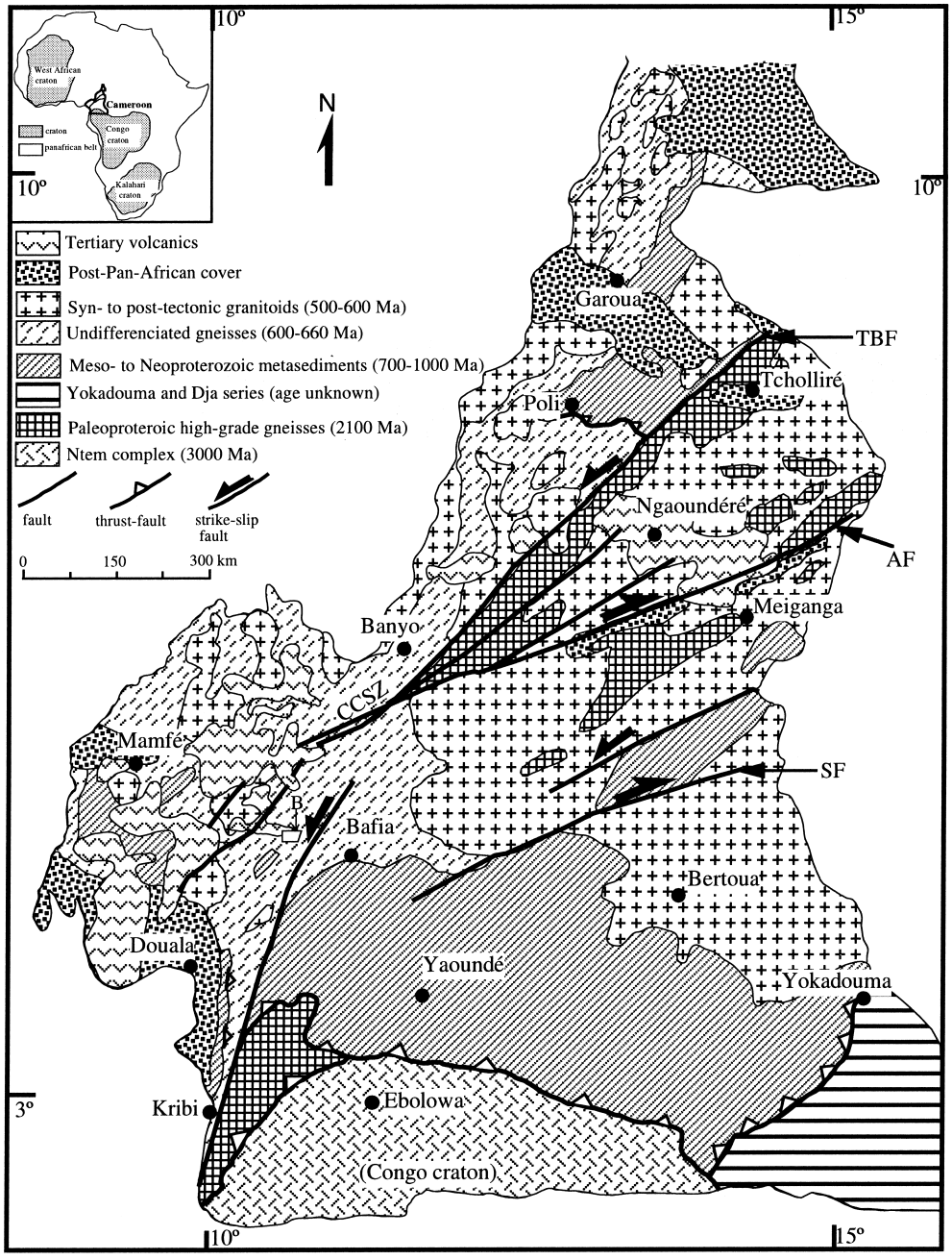

Fig. 1. Geologic sketch map of Cameroon, showing major lithotectonic units (after Soba, 1989; modified by Ngnotué et al., 2000). Ages are from Toteu et al. (2001). AF, Adamaoua fault; CCSZ, central Cameroon shear zone; SF, Sanaga fault; TBF, Tcholliré-Banyo fault. B, study area (Fig. 2).

2. Geological setting

Summarily, two major phases of deformation (D_1 and D_2) are recognized in the CAFB (Ngako *et al*., 1991; Nzenti *et al*., 1992), each of them accompanied by important magmatic activity. This magmatism is dominated by Neoproterozoic plutonism. In northern Cameroon, pre- to syn-D_1 intrusions dated at 630 Ma (U-Pb zircon; Toteu *et al*., 1987) are mainly calc-alkaline, basic to intermediate (diorites, granodiorites, tonalites) and they evoke an accretional domain. In the eastern part, Soba (1989) reported widespread diorites and peraluminous granites dated at 621–614 Ma. Syn- to late D_2 granitoids are represented by calc-alkaline to sub-alkaline anatectic granites, and syenitic and charnockitic plutons.

The D_2 structural evolution is dominated by ENE shears, among which the Adamaoua fault or Central Cameroon Shear Zone (CCSZ, Ngako *et al*., 1991) is the most important. The CCSZ is a bulk N70°E dextral wrench fault separating the CAFB in Cameroon into two main structural domains: a northern domain dominated by N-S to NW-SE trends, and a southern domain dominated by E-W structures. This lineament plays a key-role in controlling the main geometrical features of the structures of the fold belt and is assumed by Ngako *et al*. (1991, 1992) to be an ultimate consequence of an important E-W crustal shortening during the Pan-African orogenesis. Between these two structural domains the transition corresponds to a N30°E mega shear zone that is marked out in west Cameroon with, besides the numerous syntectonic Pan-African plutons, also the alignment of volcanoes and anorogenic plutons that form a part of the Cameroon volcano-tectonic line whose age range from Eocene to the present (Déruelle *et al*., 1991).

The structural evolution in the Bantoum area comprises two main phases of deformation: the phase D_1 is tangential and dominated by the schistosity and foliation planes S_1 with a mean direction N30°E, associated with a stretching lineation L_1 and isoclinal folds P_1; the phase D_2 which is observed in metamorphic formations essentially is shearing and characterized by shearing planes C_2 often filled with migmatitic leucosomes, and folds P_2 associated with an axial plane schistosity S_2. As the main structural trends in D_1 and D_2 are close (N0°–N30°E), these two deformation phases constitute probably two successive stages belonging to a single major deformation phase that has shaped the N30°E shear zone in west Cameroon. Granitoids are syn- to late-D1.

The geological map of the Bantoum area is shown in Fig. 2. The northern part is covered with tertiary basaltic trapps. The basement is essentially made up of migmatitic gneisses to which are closely associated: (1) amphibolites visible only in the form of small metric bodies or thin strips interlayered in these gneisses; (2) biotite-granites, two-mica leucogranites and quartz-monzonites occurring as concordant strips of variable widths (5 to 200 m) roughly elongated following the N70°E direction and alternating with strips of surrounding migmatitic gneisses (Fig. 3); (3) small granitic dikes crosscutting the above formations. Elongated rounded enclaves of gneisses are usual in biotite-granites (Fig. 3b), and enclaves of a mafic granulites are locally found in gneisses at the west of the study area. These formations occur mainly on mountain tops or along river beds either as isolated boulders or as large flagstones, and sometimes in small inselberg reliefs through the lateritic cover. The contacts between migmatitic

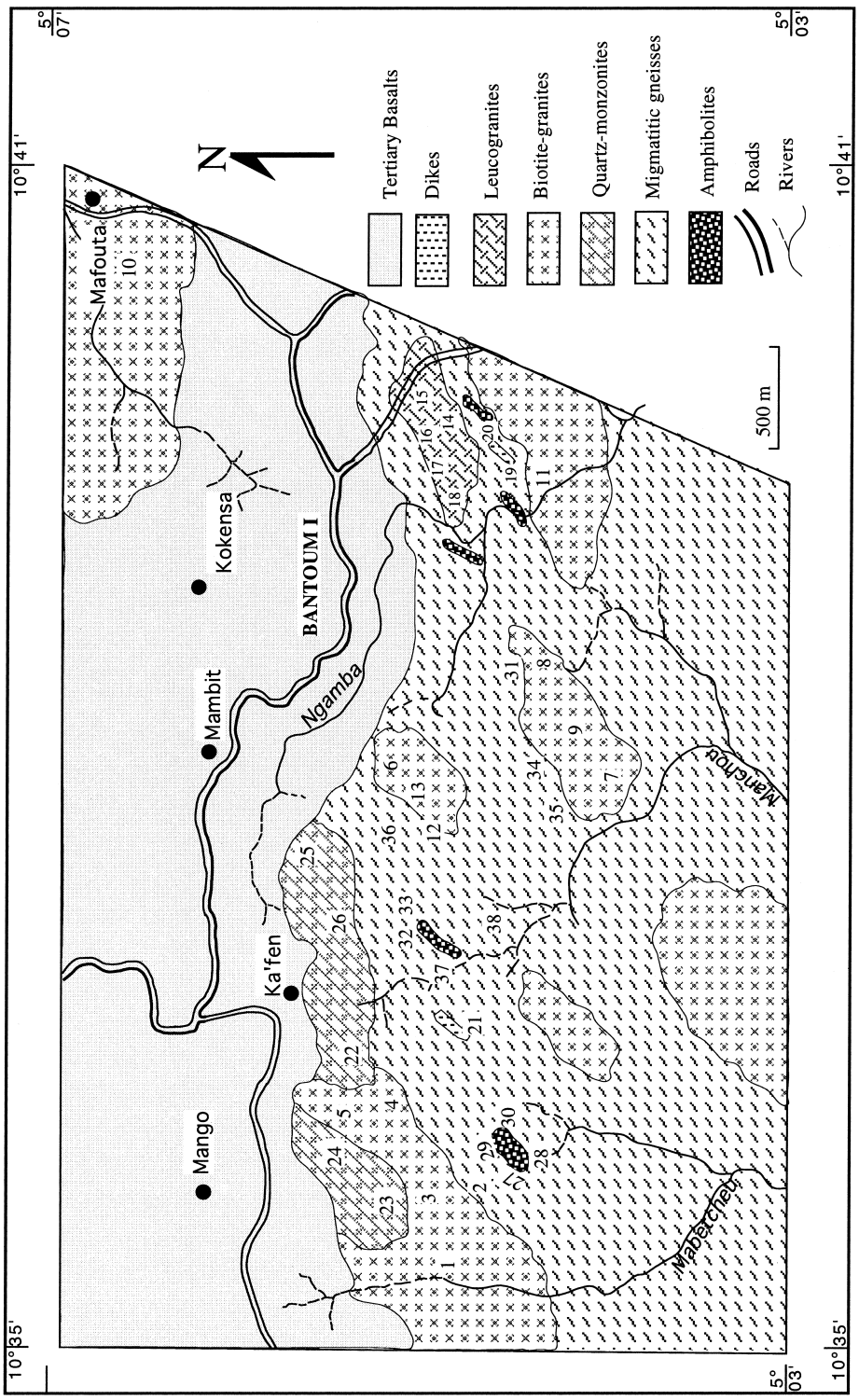

Fig. 2. Geological map of the Bantoum area, showing the locations of analyzed samples (Table 1).

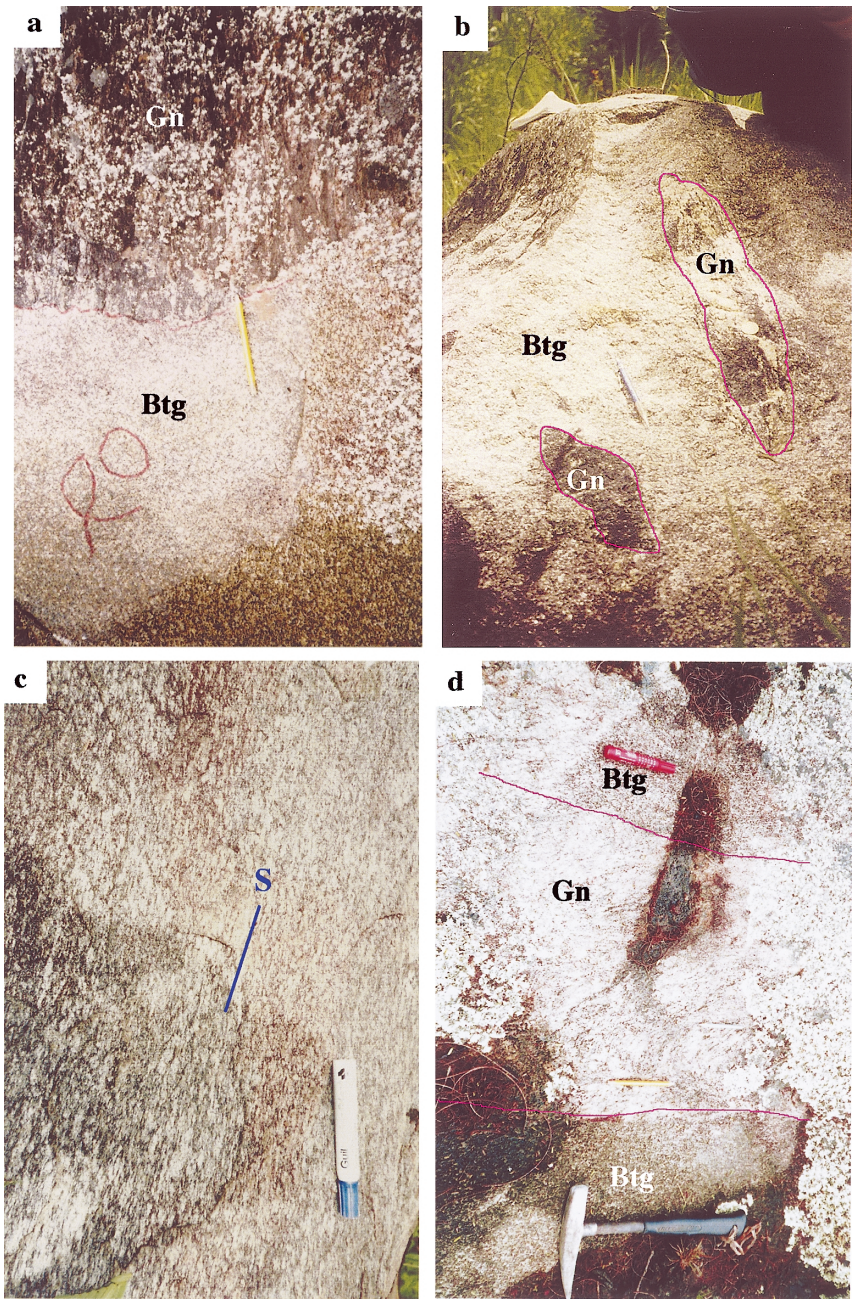

Fig. 3. Field occurrences of granitoids and gneisses in the Bantoum area. a) Contact between biotite-granite and gneiss, with same continuous foliation in both formations (the handwriting was for outcrop identification and has no meaning here). b) Biotite-granite containing elongated enclaves of migmatitic gneiss that are parallel to the foliation. c) Block of quartz-monzonite showing a strong mylonitic foliation. d) Parallel strips of biotite-granites and migmatitic gneiss. Btg, biotite-granite; Gn, gneiss; S, mylonitic foliation.

gneisses and granites are concordant and marked either by the parallelism between the migmatitic foliation and the mylonitic schistosity in the granites, or by the continuation or extension of these structures from one petrographic type to the other one (Fig. 3a). All the granitoids have undergone the same deformations as the gneisses and both share the same structural patterns; thus these granitoids deserve the appellation of "orthogneisses" as defined by Berthé *et al*. (1979) but hereafter we are still using the term granite for the sake of simplification of terminology. Since these granitoids grade into the migmatitic gneisses at the margins and are deformed along with these gneisses, and the presence of gneissic enclaves in granites we assume they could be considered as syn- to late-D_1 intrusives.

3. Petrography

Gneisses are mesocratic and medium-grained and display alternating millimeter to centimeter thick quartzo-feldspathic layers and ferro-magnesian minerals rich layers; this layering is enhanced by migmatization (metatexites) where quartzo-feldspathic leucosomes are well-developed. Their textures are predominantly granoblastic iso- or heterogranular. Amongst these gneisses, amphibole-biotite gneiss is volumetrically the most representative facies and it shows the following mineral association: quartz + K-feldspar + plagioclase(An20-22) + biotite + hornblende. At places one observes occurrence of small pink garnet crystals, that sometimes cluster to form rounded centimetric grains. Mineral association in these garnet-bearing gneisses is quartz + K-feldspar + plagioclase(An17-24) + biotite + garnet. The occurrence of plagioclase-rich gneiss is more restricted. Its mineral association is plagioclase(An31-35) + quartz + K-feldspar + biotite + garnet; here garnet occurs as small and isolated crystals. It is in this plagioclase-rich gneiss that enclaves of mafic granulites are found. Accessory minerals in all facies are zircon, allanite, apatite, titanite and opaques.

Amphibolites are granoblastic heterogranular with grain size < 4 mm. The mineral assemblage is hornblende + biotite + plagioclase(An29-35) + quartz + K-feldspar, with sphene, zircon, apatite and oxides as accessories. Hornblende forms subhedral to anhedral crystals containing inclusions of euhedral biotite, quartz and accessory minerals. Some biotite crystals include apatite, zircon and sphene. Plagioclase occurs as small subhedral crystals associated with anhedral quartz, both interstitial amidst hornblende and biotite. Sphene crystallizes in general as xenomorph rims around opaque minerals.

Mafic granulites enclaves shows dark-green melanocratic portions with granoblastic texture, essentially composed of hornblende associated with plagioclase (An91-95) and minor amount of biotite and quartz, that grade to mesocratic portions dominated by symplectitic textures comprising the association ($\pm$hornblende) + plagioclase(An98-100) + clinopyroxene + garnet + quartz and spinel-corundum corona. Accessory phases are ilmenite, magnetite, apatite and zircon.

Biotite-granites (Fig. 4a) are medium-grained and heterogranular. Due to shearing and stretching undergone by these granites, most of their main constituent minerals have been converted into fine aggregates. Porphyroclasts of more resistant minerals (usually feldspars) occur in fine-grained quartz-feldspathic matrix showing the effects of

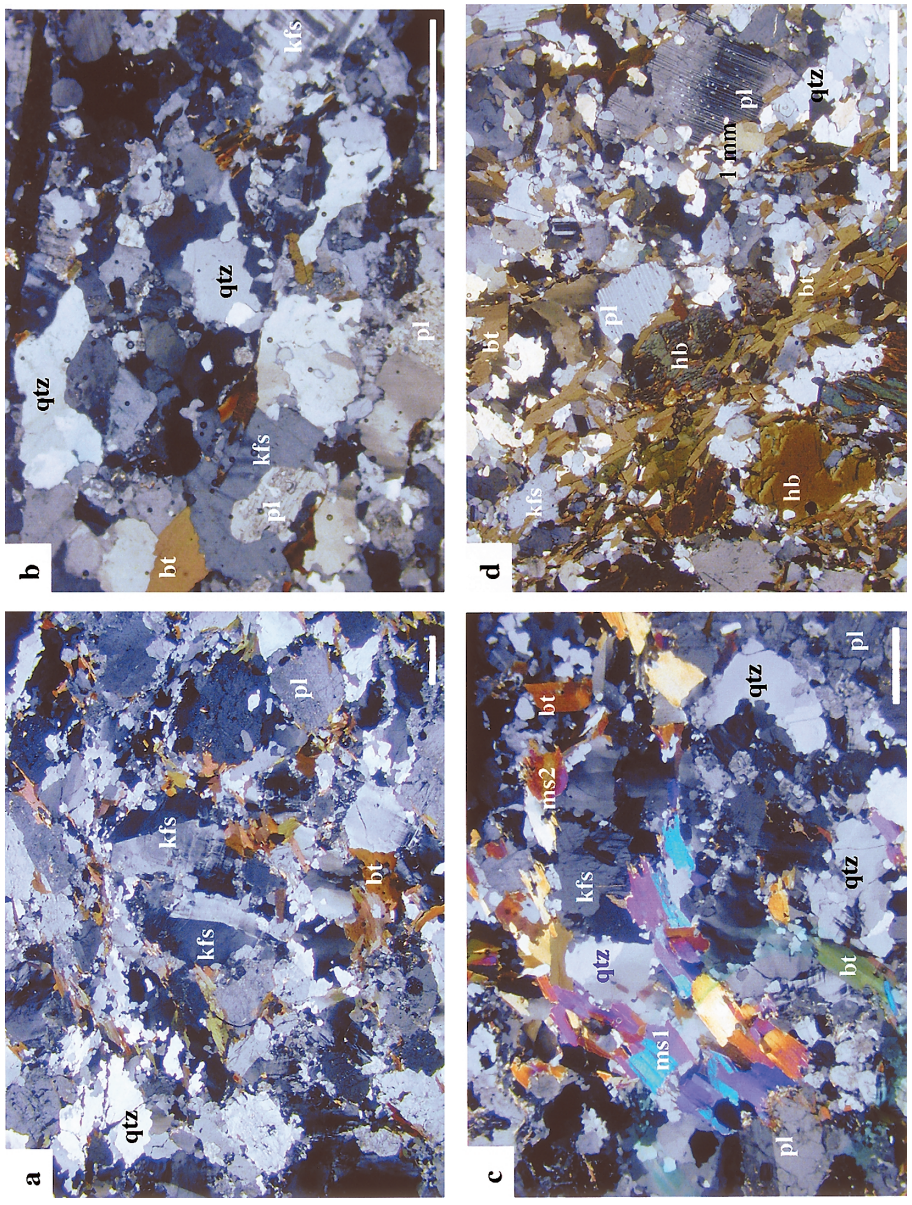

Fig. 4. Photomicrographs (crossed polars) from a) biotite-granite (sample S2.3), b) granitic dike (sample S1.4), c) leucogranite (sample S1.9b); ms1 primary, ms2 secondary muscovite, and d) quartz-monzonite (sample S4.6); all scale bars represent 1 mm. Mineral abbreviations after Kretz (1983).

dynamic recrystallization and strong preferred orientation. Myrmekitic texture is common at the borders of these large resistant crystals of feldspar in contact with recrystallized groundmass. At places primary magmatic texture is still conserved.

Biotite-granites are composed of quartz, K-feldspar, plagioclase (An23-29), biotite; accessory minerals include sphene, allanite, zircon, apatite and opaques. K-feldspar is present as microcline and orthoclase in order of abundance; crystals are dominantly subhedral, rounded or xenomorph; they are perthitic and include small biotite flakes, euhedral plagioclase and quartz. Plagioclase occurs as subhedral or rounded crystals in general elongated following the schistosity; they show sometimes undulose extinction or can be kinked. Some euhedral inclusion-free K-feldspar and plagioclase are randomly oriented, cross-cutting the schistosity. Biotite occurs as flakes of various dimensions that could be clustered, most of which have corroded margins, or as euhedral inclusions in feldspars.

Granitic dikes are fine-grained (Fig. 4b) and composed of anhedral quartz, K-feldspar, plagioclase, biotite, and muscovite. Accessory minerals (opaques, apatite and zircon) are scarce. Some ovoid plagioclase crystals are rimmed by K-feldspar. Biotite flakes in general show corroded margins and are associated with quartz-feldspathic assemblages. Muscovite is xenomorph and crystallizes at the expense of biotite and feldspar.

Two-mica leucogranite is medium-grained, exhibiting granoblastic texture with preferred orientation of feldspar, micas and quartz ribbons. K-feldspar, plagioclase (An14-16), quartz, muscovite and biotite are the main constituents, and zircon, apatite and opaques are accessory phases. K-feldspar, dominantly microcline and perthite is the most abundant mineral and occurs as subhedral to anhedral crystals; some porphyrocrysts contain inclusions of quartz, micas and plagioclase. Quartz forms either as small inclusions in other phases, or large crystals with ondulose extinction, commonly stretched or forming polycrystalline ribbons. Myrmekites are observed as small spots disseminated in some plagioclase or invading K-feldspar and plagioclase from their margins. Using the criteria of shape and relation with other neighboring phases (Lameyre, 1973; Villa *et al*., 1997), we have distinguished two generations of muscovite (Fig. 4c). Primary muscovite is the most abundant. It occurs as small euhedral inclusions or as well-shaped flakes with sharp margins and grain size ranging from 0.5 to 3.5 mm; the latter are disseminated or clustered and they include only zircon. Secondary muscovite is generally xenomorph with irregular margins growing into feldspar and biotite; they may contain inclusions of biotite, feldspar and quartz. Biotite is less abundant than muscovite.

Quartz-monzonites (Fig. 4d) are leucocratic and fine- to medium-grained showing granoblastic texture. Plagioclase (An30-38) forms either anhedral grains intergrowing with other phases, or big subhedral elongated crystals usually surrounded with small groundmass crystals. K-feldspar is in general rounded, with inclusions of plagioclase, biotite, quartz, apatite and zircon; some ones are perthitic. Biotite flakes are usually aggregated around feldspars or are associated with hornblende to form mafic clusters. Quartz is interstitial or occurs as polycrystalline recrystallized grains. Sphene could be euhedral or xenomorph, forming rims around and also intergrowth with opaques; other accessories are zircon, acicular apatite, allanite and secondary epidote growing at the

expense of hornblende.

4. Geochemistry

4.1. Analytical procedures

Samples weighing 0.5–1.5 kg were reduced and finely chipped. Afterwards, they were cleaned four times using an ultrasonic bath with ultrapure water. Sample chips were crushed by hand in a tungsten carbide mill, split by quartering and finely ground. For some samples, analyses of major and trace elements (including REE) have been performed by ICP-MS at CRPG (Nancy, France). For other samples, major and trace element (without REE) concentrations have been done by XRF spectrometry using Rigaku RIX 3000 at the Faculty of Science, Niigata University. They were determined from fused glass beads prepared with both anhydrous lithium tetraborate ($Li_2B_4O_7$) and lithium metaborate ($LiBO_2$) flux, with a sample to flux ratio of 1:2. A maximum error of 5% is estimated for the Rb/Sr ratio, based on the reproducibility of the data for the Geological Survey of Japan standard JB-1a.

All the isotope analyses were carried out using a Finigan MAT 262 thermal ionization mass spectrometer equipped with nine Faraday cup collectors at the Faculty of Science, Niigata University. Rb-Sr and Sm-Nd extraction and mass spectrometric analyses were made following the procedures described by Kagami *et al*. (1987).

Measured $^{87}Sr/^{86}Sr$ and $^{143}Nd/^{144}Nd$ ratios were normalized to $^{86}Sr/^{88}Sr=0.1194$ and $^{146}Nd/^{144}Nd=0.7219$ respectively. Whole procedure blanks were 0.55 ng Sr, 0.04 ng Sm and 0.40 ng Nd, and then their influence on the isotope ratios of measured samples are considered to be negligible. Rb-Sr concentrations are those of XRF analyses. Sm-Nd concentrations were measured using $^{149}Sm/^{150}Nd$ mixed spikes.

The $^{87}Sr/^{86}Sr$ ratios for this study are reported relative to 0.710242 for the NBS987 (Kagami *et al*., 1987) and $^{143}Nd/^{144}Nd$ ratios relative to GSJ standard JNdi-1 = 0.512116 that is consistent with 0.511858 of LaJolla (Tanaka *et al*., 2000). The $^{143}Nd/^{144}Nd$ ratios for the JNdi-1 standard were measured six times and varied from 0.512080 $\pm$0.000012 (2σ) to 0.512094$\pm$0.000012 (2σ).

Rb-Sr isochron ages are calculated using a personal computer program of Kawano (1994) which is based on the equation of York (1966) with the following decay constants: $\lambda(^{87}Rb)=1.42\times10^{-11}y^{-1}$ (Steiger and Jäger, 1977) and $\lambda(^{147}Sm)=6.54\times10^{-12}y^{-1}$ (Lugmair and Marti, 1978). Standard errors used for $^{87}Sr/^{86}Sr$, $^{87}Rb/^{86}Sr$, $^{147}Sm/^{144}Nd$ and $^{143}Nd/^{144}Nd$ ratios calculation are 0.01% (1σ), 5% (1σ), 0.1% (1σ), and 0.01% (1σ) respectively.

Model ages and ε_{Nd} values were calculated using values of present-day depleted mantle defined by Goldstein *et al*. (1984): $^{143}Nd/^{144}Nd$ (present) = 0.51315 and $^{147}Sm/^{144}Nd$ (present) = 0.2136. The following CHUR parameters were used for calculations of initial ε_{Sr} and initial ε_{Nd} values: $^{87}Sr/^{86}Sr$ (present) = 0.7045, $^{87}Rb/^{86}Sr$ (present) = 0.0827, $^{143}Nd/^{144}Nd$ (present) = 0.512638 and $^{147}Sm/^{144}Nd$ (present) = 0.1966 (Goldstein *et al*., 1984).

4.2. Major elements

Major elements data for some representative samples of gneisses and granitoids of

Table 1. Representative analyses of gneisses and granitoids from the Bantoum area. Analyses performed by ICP-MS (samples with REE data) or XRF (samples without REE data).

	Biotite-granites I									
	1	2	3	4	5	6	7	8	9	10
Sample	B462	S4.5b	S4.3	S4.5	B46	S3.8	S2.5	S2.3	B24	BOO
SiO_2 wt%	64.92	68.27	69.99	68.41	68.71	70.40	71.11	71.23	71.34	72.59
TiO_2	0.84	0.58	0.41	0.60	0.60	0.47	0.50	0.54	0.48	0.23
Al_2O_3	16.16	15.07	14.39	15.34	15.54	14.45	13.78	13.99	14.03	13.91
Fe_2O_3*	4.92	2.87	2.27	3.20	3.17	2.96	3.44	3.52	2.98	2.36
MnO	0.05	0.03	0.02	<L.D.	0.03	0.03	0.04	0.03	<L.D.	0.02
MgO	1.04	0.72	0.51	0.81	0.80	0.63	0.73	0.76	0.65	0.18
CaO	2.42	1.53	1.33	1.65	1.50	1.42	1.38	1.57	1.53	1.06
Na_2O	3.47	3.06	2.88	3.02	3.07	2.71	2.92	2.92	2.86	3.29
K_2O	4.92	6.15	6.08	6.02	6.02	5.69	5.09	4.72	5.33	5.58
P_2O_5	0.29	0.27	0.16	0.21	0.25	0.16	0.20	0.20	0.16	0.14
L.O.I.	0.52	0.76	0.72	0.73	0.56	0.46	0.61	0.60	0.51	0.30
Total	99.55	99.31	98.75	99.99	100.25	99.38	99.80	100.08	99.87	99.66
K_2O/Na_2O	1.42	2.01	2.11	1.99	1.96	2.10	1.74	1.62	1.86	1.70
Na_2O+K_2O	8.39	9.21	8.96	9.04	9.09	8.40	8.01	7.64	8.19	8.87
T°C Zr	828	825	808	835	839	813	823	828	812	817
Ba ppm	1126	1361	1000	1495	1251	830	715	600	781	424
Cr	8.5	8	13	6.9	6.8	<L.D.	5.3	5.8	<L.D.	1.0
Ga	26.8	-	-	26.9	25.4	22.7	24.3	26.4	23.3	-
Hf	7.67	-	-	11.4	10.3	7.53	7.62	8.05	6.49	-
Nb	29	15	17	17	16	19	23	29	18	38
Ni	5.9	8	8	10.2	8.6	<L.D.	8.1	6.2	<L.D.	17
Rb	199	216	232	217	215	202	180	183	199	246
Sr	281	266	205	244	241	212	182	180	191	102
Ta	2.00	-	-	0.91	0.63	1.24	0.83	0.78	0.94	-
Th	29.9	-	-	75.5	72.7	32.6	54.8	58.4	41.3	-
V	63.3	42	36	49.0	47.2	30.2	34.6	37.6	30.8	11
Y	23.1	24.5	101	29.2	9.5	17.4	26.9	83.1	16.98	55
Zn	105	89	-	110	95.2	68.8	88.3	93.0	73.8	67
Zr	371	352	281	383	381	275	298	309	277	290
										-
La ppm	98.3	-	-	179	149	71.6	115	120	92.9	-
Ce	190	-	-	353	307	133	160	203	176	-
Pr	21.2	-	-	41.1	34.6	15.3	21.5	22.7	18.9	-
Nd	76.0	-	-	145	124	51.3	74.6	79.7	64.6	-
Sm	12.1	-	-	19.1	15.7	7.78	10.5	12.2	9.32	-
Eu	1.65	-	-	2.08	1.83	1.34	1.45	1.43	1.33	-
Gd	8.27	-	-	8.82	7.45	5.23	6.41	11.1	5.08	-
Tb	1.00	-	-	0.96	0.71	0.64	0.86	1.57	0.66	-
Dy	4.99	-	-	3.72	2.60	3.26	4.00	9.11	3.05	-
Ho	0.79	-	-	0.59	0.28	0.57	0.70	1.91	0.53	-
Er	2.08	-	-	2.12	0.88	1.66	1.91	5.63	1.48	-
Tm	0.24	-	-	0.35	0.08	0.21	0.23	0.80	0.22	-
Yb	1.46	-	-	2.05	0.47	1.45	1.27	4.97	1.16	-
Lu	0.19	-	-	0.33	0.08	0.21	0.22	0.81	0.20	-

Table 1 (Continued).

	Biotite-granites II			Leucogranites					Granitic dikes		
	11	12	13	14	15	16	17	18	19	20	21
Sample	S1.1	S3.3b	S3.3b2	B151	B152	B15	S1.9a	S1.9b	S1.42	S1.4	S14n
SiO_2 wt%	75.62	76.62	77.14	73.96	74.08	74.35	74.14	73.86	72.79	72.89	73.54
TiO_2	0.22	0.12	0.16	0.15	0.15	0.16	0.11	0.18	0.24	0.23	0.24
Al_2O_3	11.88	11.85	11.43	14.10	14.38	14.08	14.41	14.68	14.27	14.37	14.26
Fe_2O_3*	2.81	1.85	2.68	1.61	1.47	1.46	1.03	1.94	1.81	1.77	1.52
MnO	0.04	0.03	0.03	<L.D.	<L.D.	0.02	0.01	0.03	<L.D.	<L.D.	0.01
MgO	0.16	0.00	<L.D.	0.17	0.18	0.14	0.07	0.16	0.29	0.25	0.27
CaO	0.78	0.67	0.78	0.83	0.89	0.63	0.63	0.72	0.71	0.71	0.72
Na_2O	2.42	2.21	2.15	3.04	3.22	2.78	3.12	2.74	3.00	3.05	3.19
K_2O	5.35	6.01	5.49	5.41	5.38	6.04	5.52	4.78	6.34	6.44	6.28
P_2O_5	0.05	0.03	<L.D.	0.06	0.09	0.08	0.08	0.13	0.14	0.09	0.14
L.O.I.	0.50	O,55	0.44	0.44	0.58	0.66	0.89	1.01	0.57	0.46	0.56
Total	99.83	99.94	100.30	99.77	100.42	100.42	100.01	100.23	100.16	100.26	100.72
K_2O/Na_2O	2.21	2.72	2.55	1.78	1.67	2.17	1.77	1.74	2.11	2.11	1.97
Na_2O+K_2O	7.77	8.22	7.64	8.45	8.60	8.83	8.64	7.52	9.34	9.49	9.47
T°C Zr	866	846	851	742	745	740	719	736	753	751	752
Ba ppm	372	119	123	127	145	175	112	63.5	380	372	4070
Cr	<L.D.	7.0	<L.D.	<L.D.	<L.D.	8	0	6.7	<L.D.	<L.D.	9
Ga	23.6	-	25.9	29.4	31.0	-	-	-	21.9	22.0	-
Hf	12.0	-	14.08	3.55	3.91	-	-	-	4.01	4.04	-
Nb	29	22	24	21	21	21	24	36	10	11	12
Ni	<L.D.	2	<L.D.	<L.D.	<L.D.	<L.D.	6	13	<L.D.	<L.D.	<L.D.
Rb	135	158	132	346	367	370	386	390	237	244	257
Sr	60.1	30.0	24.8	35.6	42.0	45.5	33.0	21.5	87.2	88.3	97.3
Ta	2.19	-	0.49	1.19	1.26	-	-	-	0.50	0.49	-
Th	14.7	-	21.7	33.6	32.5	-	-	-	31.7	31.7	-
V	8.4	7	<L.D.	<L.D.	<L.D.	4	7	7	4.7	4.7	7
Y	108	69	81.3	16.3	16.2	13	19	22	33.2	32.4	43
Zn	70.9	51	65.6	79.8	78.8	-	55	108	61.1	64.1	-
Zr	446	386	393	104	109	103	74	79	130	135	133
		-				-	-	-	-	-	-
La ppm	96.2	-	124	34.8	32.5	-	-	-	52.7	50.3	-
Ce	207	-	247	71.2	65.4	-	-	-	88.9	86.1	-
Pr	24.5	-	29.4	8.35	7.64	-	-	-	10.9	10.6	-
Nd	94.6	-	113	29.6	28.0	-	-	-	40.8	39.2	-
Sm	21.6	-	24.4	6.87	6.34	-	-	-	8.99	8.77	-
Eu	1.35	-	0.96	0.42	0.48	-	-	-	0.85	0.88	-
Gd	21.4	-	21.6	4.75	4.76	-	-	-	8.45	8.45	-
Tb	3.33	-	3.31	0.69	0.65	-	-	-	1.12	1.06	-
Dy	19.5	-	18.2	2.92	2.87	-	-	-	5.17	5.17	-
Ho	3.83	-	3.24	0.49	0.49	-	-	-	1.02	0.94	-
Er	9.98	-	7.58	1.17	1.06	-	-	-	2.54	2.15	-
Tm	1.34	-	0.92	0.12	0.12	-	-	-	0.30	0.28	-
Yb	7.96	-	5.03	0.69	0.71	-	-	-	1.66	1.63	-
Lu	1.00	-	0.71	0.11	0.08	-	-	-	0.26	0.25	-

Table 1 (Continued).

	Quartz-monzonites				Plagioclase-rich gneiss				
	22	23	24	25	26	27	28	29	30
Sample	B47	S4.7	S4.6	S3.6	S3.7c	S4.1	S4.1a	S4.1j	B43
SiO_2 wt%	54.29	55.18	55.17	57.41	57.72	63.10	66.99	62.39	65.99
TiO_2	1.89	1.84	1.79	1.46	1.39	1.16	1.13	1.38	1.16
Al_2O_3	16.63	15.90	15.77	16.18	16.13	14.47	13.78	14.80	14.14
Fe_2O_3*	9.09	8.32	8.23	8.06	7.84	7.28	7.13	8.88	7.37
MnO	0.12	0.11	0.10	0.10	0.11	0.14	0.15	0.15	0.16
MgO	3.26	3.02	3.26	3.52	3.61	2.63	1.18	2.04	1.32
CaO	5.48	5.09	5.10	5.22	5.04	5.01	3.29	4.58	3.53
Na_2O	3.34	3.19	3.35	3.19	3.29	3.29	3.16	3.30	3.24
K_2O	4.38	4.51	4.34	3.58	3.70	1.85	2.14	1.99	2.08
P_2O_5	0.95	1.10	1.07	0.48	0.47	0.30	0.33	0.29	0.34
L.O.I.	0.66	0.69	0.61	0.81	0.58	0.51	0.30	0.12	0.26
Total	100.09	98.94	98.79	100.01	99.88	99.74	99.58	99.92	99.58
K_2O/Na_2O	1.31	1.41	1.30	1.12	1.12	0.56	0.68	0.60	0.64
Na_2O+K_2O	7.72	7.70	7.69	6.77	6.99	5.14	5.30	5.29	5.32
T°C Zr	753	760	763	768	757				
Ba ppm	2020	2134	2393	1493	1269	646	1198	746	1090
Cr	39.6	45	55	98.7	91.6	62	7	53.3	16
Ga	24.2	-	-	22.9	22.6	-	-	25.7	-
Hf	8.28	-	-	7.91	6.92	-	-	7.71	-
Nb	28	31	23	25	24	18	20	20	21
Ni	26.6	22	37	47.0	48.7	24	9	28.0	8
Rb	173	171	161	196	148	54	75	62	74
Sr	1102	1042	1069	609	548	237	297	290	306
Ta	1.74	-	-	1.53	1.65	-	-	1.53	-
Th	17.0	-	-	18.4	17.4	-	-	9.71	-
V	153	169	146	133	122	103	39	101	59
Y	26.1	27	28	20.5	18.5	54	55	52.7	54
Zn	139	-	106	114	112	88	79	117	-
Zr	346	357	378	324	282	329	426	333	392
La ppm	107	-	-	96.3	79.7	-	-	18.3	-
Ce	211	-	-	192	145	-	-	79.1	-
Pr	23.7	-	-	20.4	16.8	-	-	6.22	-
Nd	92.4	-	-	75.0	62.6	-	-	26.6	-
Sm	14.3	-	-	11.0	9.74	-	-	7.20	-
Eu	3.62	-	-	2.49	2.19	-	-	2.51	-
Gd	9.47	-	-	7.74	6.15	-	-	8.29	-
Tb	1.20	-	-	0.93	0.90	-	-	1.38	-
Dy	5.99	-	-	4.55	4.37	-	-	8.61	-
Ho	0.89	-	-	0.66	0.68	-	-	1.83	-
Er	2.22	-	-	1.71	1.77	-	-	4.96	-
Tm	0.26	-	-	0.21	0.22	-	-	0.73	-
Yb	1.75	-	-	1.37	1.37	-	-	4.86	-
Lu	0.27	-	-	0.23	0.21	-	-	0.68	-

Table 1 (Continued).

	Hornblende-biotite gneiss							
	31	32	33	34	35	36	37	38
Sample	B21	S3.5c	B31	B25	S2.62	S3.1	S3.11	S3.12
SiO_2 wt%	71.12	76.60	77.52	69.03	70.11	78.64	73.68	71.76
TiO_2	0.26	0.28	0.28	0.36	0.39	0.14	0.37	0.17
Al_2O_3	14.60	10.99	11.00	14.70	13.88	11.23	12.67	13.57
Fe_2O_3*	4.25	3.33	3.26	4.36	4.39	2.22	2.98	3.22
MnO	0.06	0.11	0.10	0.05	0.08	0.03	0.05	0.09
MgO	<L.D.	1.10	0.05	0.24	0.23	0.02	0.31	0.01
CaO	1.16	0.94	1.02	1.59	1.36	1.11	0.98	1.12
Na_2O	3.95	2.14	2.25	3.03	3.43	2.90	2.72	2.56
K_2O	4.20	4.60	4.36	5.94	5.43	3.42	5.29	6.57
P_2O_5	0.09	0.04	0.03	0.08	0.10	0.02	0.12	0.04
L.O.I.	0.66	0.46	0.24	0.43	0.33	0.44	0.32	0.57
Total	100.35	100.59	100.10	99.81	99.73	100.17	99.49	99.68
K_2O/Na_2O	1.06	2.15	1.93	1.96	1.58	1.18	1.94	2.57
Na_2O+K_2O	8.15	6.74	6.61	8.97	8.86	6.32	8.01	9.13
T°C Zr								
Ba ppm	435	877	1001	784	766	142	549	239
Cr	<L.D.	1	14	<L.D.	19	53	4	0
Ga	39.4	-	-	35.6	-	-	-	-
Hf	20.58	-	-	13.30	-	-	-	-
Nb	83	40	43	68	87	19	38	60
Ni	<L.D.	16	<L.D.	<L.D.	15	8	3	12
Rb	241	176	145	182	170	111	166	156
Sr	46.1	91	90	86.8	90	51	136	44
Ta	2.46	-	-	2.02	-	-	-	-
Th	16.2	-	-	18.4	-	-	-	-
V	<L.D.	7	5	3.5	8	7	18	7
Y	105	103	71	66.9	116	65	68	164
Zn	149	80	-	92.6	93	53	75	115
Zr	840	559	572	541	562	339	488	646
La ppm	87.6	-	-	113	-	-	-	-
Ce	195	-	-	219	-	-	-	-
Pr	21.4	-	-	25.2	-	-	-	-
Nd	79.3	-	-	88.4	-	-	-	-
Sm	17.5	-	-	17.0	-	-	-	-
Eu	1.42	-	-	1.82	-	-	-	-
Gd	15.8	-	-	15.9	-	-	-	-
Tb	2.80	-	-	2.37	-	-	-	-
Dy	17.5	-	-	13.9	-	-	-	-
Ho	3.59	-	-	2.70	-	-	-	-
Er	9.37	-	-	6.77	-	-	-	-
Tm	1.33	-	-	0.82	-	-	-	-
Yb	8.03	-	-	4.78	-	-	-	-
Lu	1.06	-	-	0.60	-	-	-	-

* total iron as Fe_2O_3; L.O.I. loss on ignition; <L.D. below the limit of detection; - not analyzed

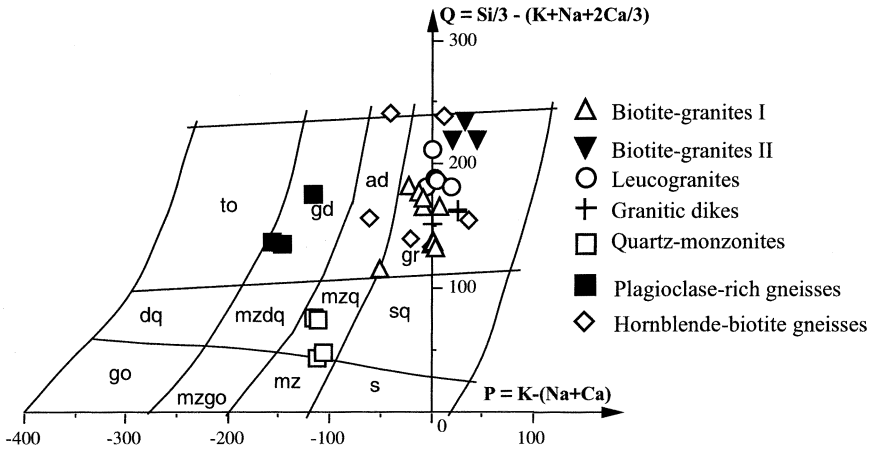

Fig. 5. Position of the Bantoum granitoids and gneisses in the P=Si/3−(K+Na+2Ca/3) vs P=K−(Na+Ca) (gram-atoms×10³) multicationic nomenclature diagram of igneous rocks after Debon and Le Fort (1983). gr, granite; ad, adamellite; gd, granodiorite; to, tonalite; sq, quartz-syenite; mzq, quartz-monzonite; mzdq, quartz-monzodiorite; dq, quartz-diorite; s, syenite; mz, monzonite; mzgo, monzodiorite; go, gabbro.

the Bantoum area are listed in Table 1. We used the P=K−(Na+Ca) vs. Q=Si/3−(K+Na+2Ca/3) multi-cationic diagram of Debon and Le Fort (1983) for nomenclature chemical composition of the different petrographic types, as this diagram takes into account the main major elements. Biotite-granites, granitic dike, leucogranites and hornblende-biotite gneisses share the granitic field (Fig. 5); plagioclase-rich gneiss has a granodioritic composition. SiO_2 contents range from 56–58 wt% in quartz-monzonites and 65 to 77 wt% for other granites; the gap between 56–65 wt% silica content is noticeable. In the Harker diagrams (Fig. 6), the most felsic samples (75–77 wt% SiO_2) amongst biotite-granites show some slight chemical differences with other terms, in particular their much lower content in MgO, CaO, TiO_2, Al_2O_3 and Na_2O. Hereafter we refer to the less felsic biotite-granites as "granites I" and more felsic ones as "granites II", even though they show no significant difference on the field. All granitoids have high total alkali contents ($6.8\% < Na_2O + K_2O < 9.5\%$). They are hyperpotassic (K_2O = 3.6–6.4 wt%), having K_2O/Na_2O ratios ranging from 1.1 to 2.7 with lowest values in quartz-monzonites (1.1–1.4). High TiO_2 contents (1.46–1.89 wt%) in quartz-monzonites could be explained by the abundance of sphene (up to 3 vol% in some samples). Regarding the Al saturation index (A/CNK = molar $Al_2O_3/(CaO+Na_2O+K_2O)$), quartz-monzonites are metaluminous while biotite-granites and granitic dikes are slightly peraluminous and leucogranites are peraluminous. In the A/CNK *vs* SiO_2 diagram (Fig. 7), only leucogranites plot in the field of S-type granites and other granites are in the field of I-type granitoids (Chappell and White, 1992). In the (Na_2O+K_2O) *vs* SiO_2 and AFM diagrams (Fig. not shown) they show a calc-alkaline trend. In addition the presence of normative corundum in leucogranites (1.9–4%) and biotite-granites (0.6–1.3%) and their absence in quartz-monzonites supports this subdivision.

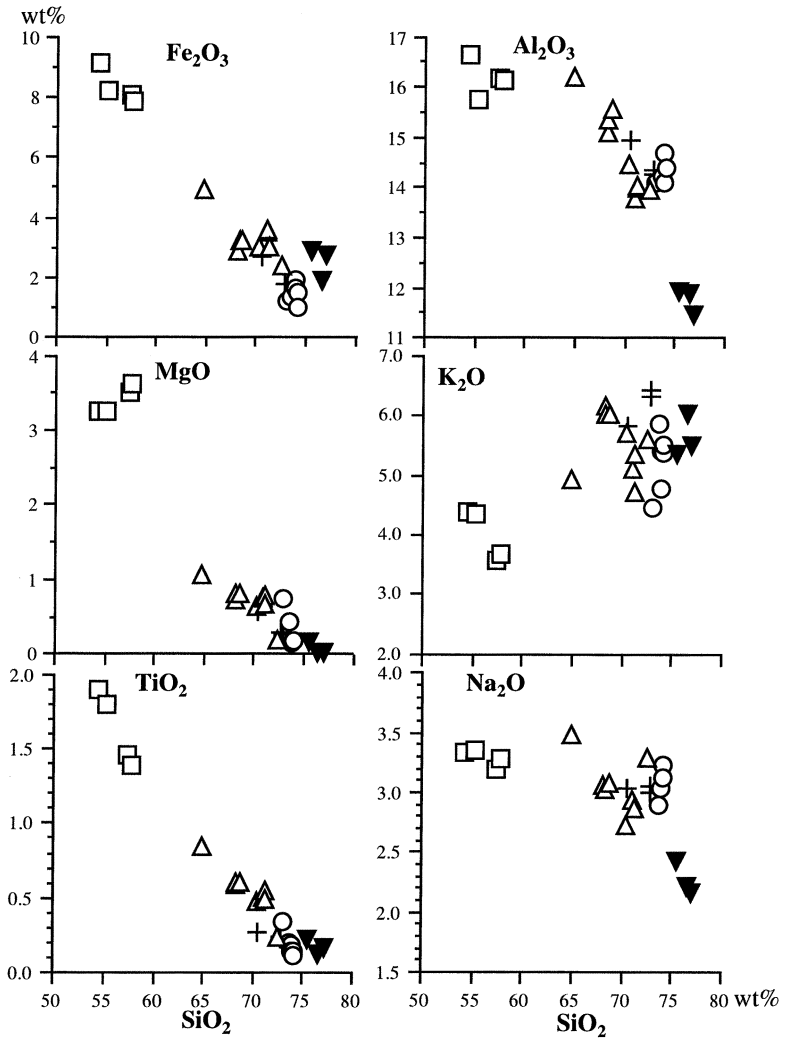

Fig. 6. Harker variation diagrams for some selected major elements. Symbols as in Fig. 5.

4.3. Trace elements

The trace element contents of Bantoum granitoids and gneisses are reported in Table 1. Although they are in general scattered on variation diagrams (Fig. 8), some features are noteworthy. Ba abundance is high in quartz-monzonites (1268–2393 ppm), moderate in granites I and dikes (371–1495 ppm) and low in granites II and leucogranites (63–372 ppm). Ba/Sr ratios range between 1.8–2.5 in quartz-monzonites and are alike in other groups (3–6). Rb/Ba <1 except in leucogranites (2.5–6.1); likewise Rb/Sr ratios are much higher in leucogranites (8.7–18.1) than in biotite-granites and granitic dikes (0.7–2.8) and quartz-monzonites (<0.4). K/Rb ratios are also significantly lower in leucogranites (126–156) compared to quartz-monzonites and

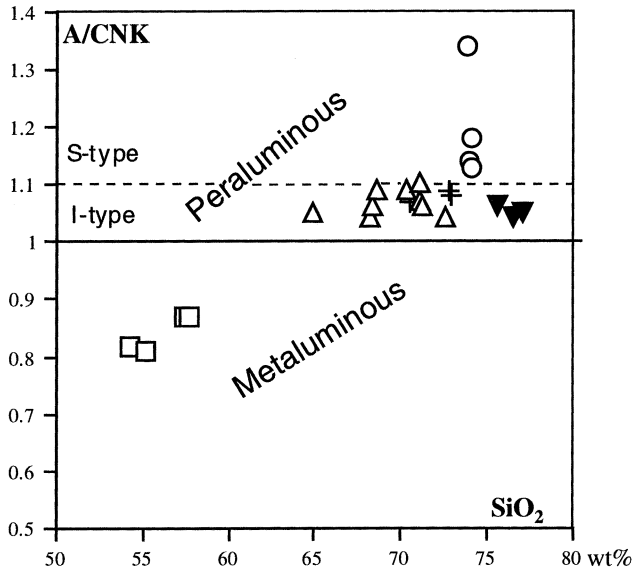

Fig. 7. Molar $Al_2O_3/(CaO+Na_2O+K_2O)$ vs SiO_2 diagram for the Bantoum granitoids. Boundary between I-type and S-type according to Chappell and White (1992). Symbols as in Fig. 5.

biotite-granites (247–416); these values are similar to those observed in continental calc-alkaline igneous suites (*e.g.* Bertrand *et al*., 1984; Ayuso and Arth, 1992).

Trace elements distribution patterns show that all these rocks have a distinctive depletion in Nb, Ta, Sr and Ti (except quartz-monzonites) relative to other trace elements, and are enriched in LILE (large ion lithophile elements) compared to anomalies in Sr, Ba and Ti; and distinctively higher contents of Th are observed in the biotite-granites I. Quartz-monzonites display less pronounced negative anomalies in Sr and Ti, and lower Rb, Y and Yb values resulting in more "fractionated" trace element distribution pattern, characteristic of calc-alkaline arc granitoids. Also noticeable is the similarity between trace elements distribution patterns of biotite-granites II and hornblende-biotite gneisses (Fig. 9d). Overall, the enrichment in the incompatible elements (K, Rb, Ba) and depletion in high field strength elements (HFSE) supports the importance of the crustal source component in the genesis of the Bantoum granitoids.

The conventional tectonic discrimination diagrams of Pearce *et al*. (1984; Fig. 10) are used to summarize some of the salient trace element geochemical features of the Bantoum gneisses and granites. Leucogranites have trace element compositions which straddle the field boundary between volcanic arc granites and syn-collisional granites. High Rb/Zr ratios (3–5) and lower K/Rb ratios of the leucogranites support their syn-collisional characters (Harris *et al*., 1986). Quartz-monzonites, granites I and granitic dikes plot within the field of volcanic arc granitoids, whereas "granites II" and both hornblende-biotite and plagioclase-rich gneisses plot within the within plate granitoids field.

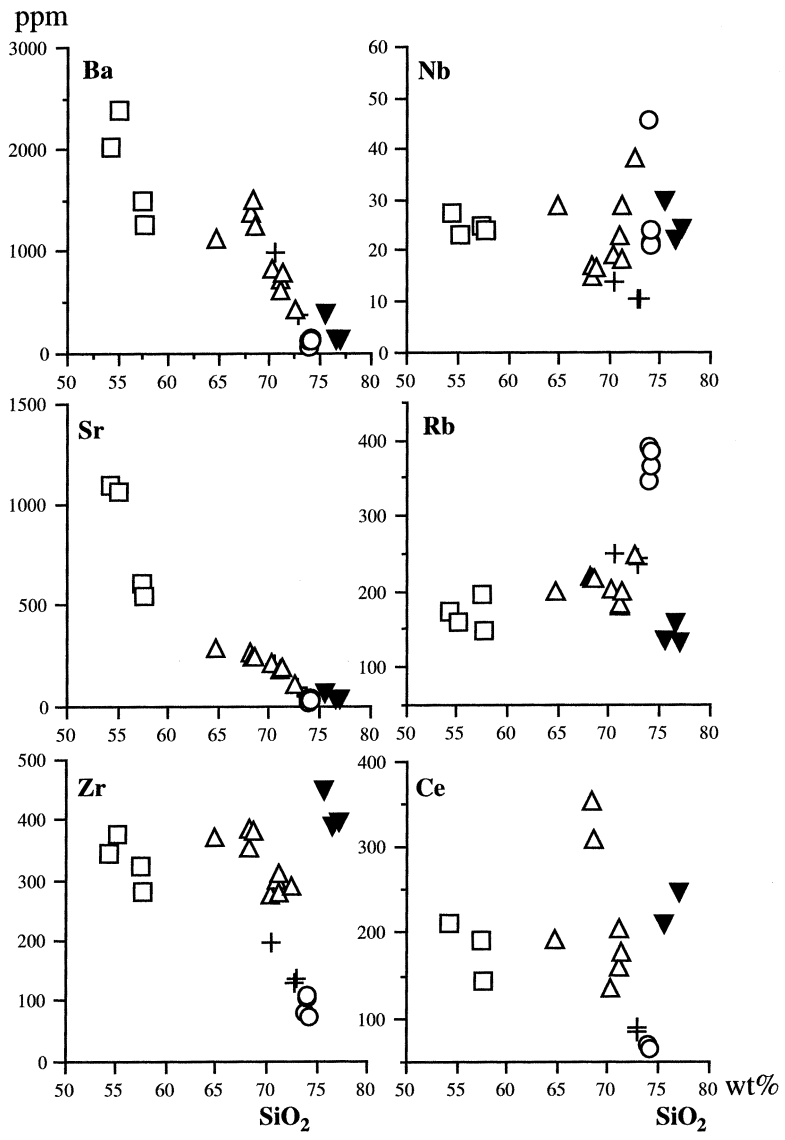

Fig. 8. Variation diagrams for some trace elements in the Bantoum granitoids. Symbols as in Fig. 5.

4.4. Rare earth elements

Total REE is lower (151–224 ppm) in leucogranites and granitic dikes comparatively to both biotite-granites I and II and quartz-monzonites (294–757 ppm). Chondrite-normalized REE patterns (Fig. 11) in general indicate strong LREE enrichment but variable LREE/HREE contents ($La_N/Yb_N = 8–61$). Quartz-monzonites and biotite-granites I display similar consistent fractionation trend within the LREE and HREE groups ($La_N/Yb_N = 33–61$; $La_N/Sm_N = 5–7$ and $Gd_N/Yb_N = 3–5$; $Ce_N/Yb_N = 23–44$), except for two samples (B46 and S2.3) of granites I that are significantly much more

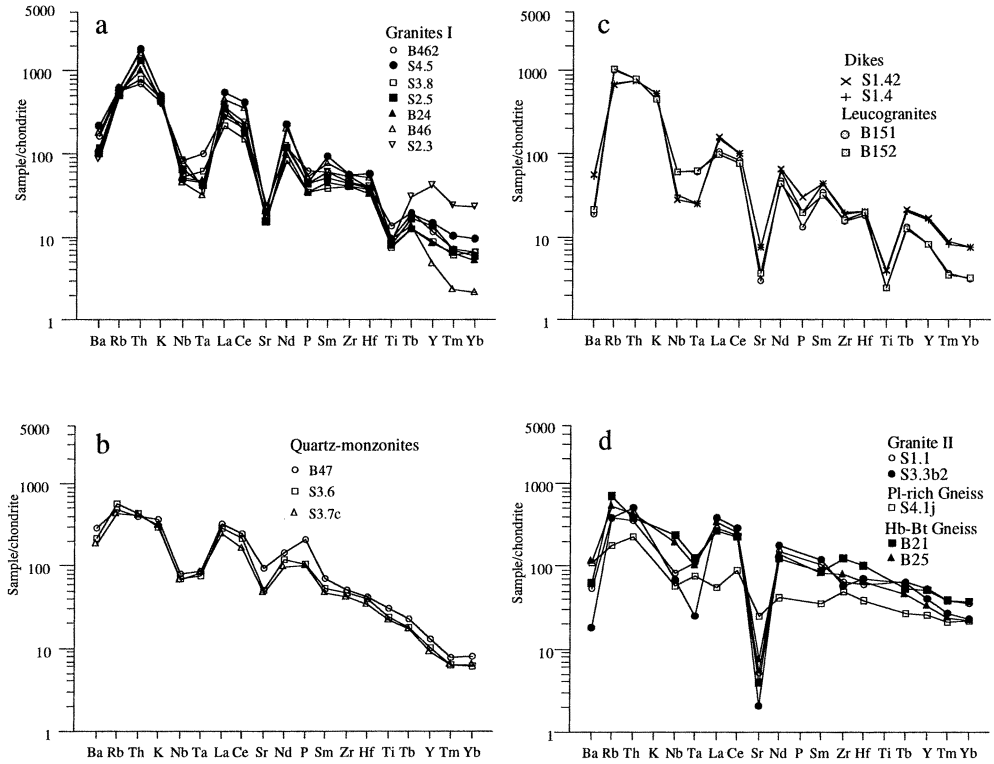

Fig. 9. Chondrite-normalized trace-element distribution for the Bantoum granitoids and gneisses. Normalization values after Thompson et al. (1984).

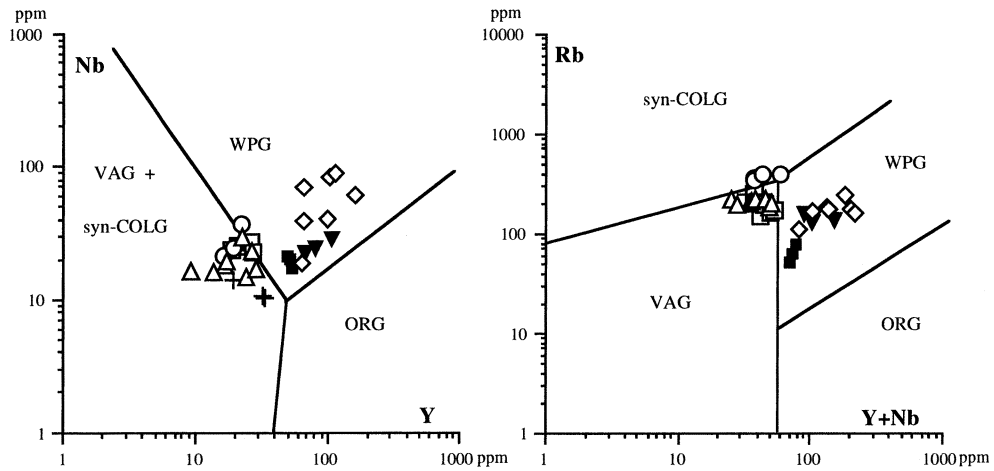

Fig. 10. Nb vs Y and Rb vs Y+Nb discrimination diagrams (Pearce et al., 1984) for the granites and gneisses of Bantoum area. WPG, Within-Plate Granites; VAG, Volcanic Arc Granites; syn-COLG, syn-Collisional Granites; ORG, Oceanic Ridge Granites. Symbols as in Fig. 5.

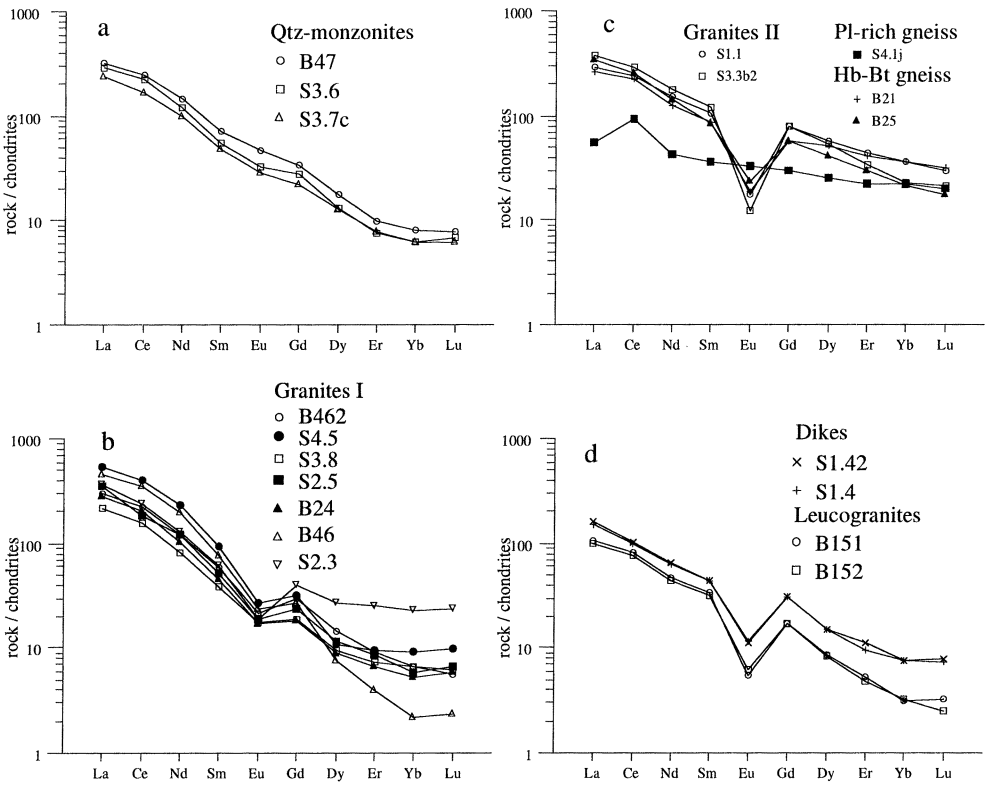

Fig. 11. Chondrite-normalized rare earth element patterns for the Bantoum granitoids and amphibole-biotite gneisses. Normalization values after Nakamura (1974).

fractionated in HREE ($Gd_N/Yb_N = 13$ and $La_N/Yb_N = 210$) and less fractionated ($Gd_N/Yb_N = 2$ and $La_N/Yb_N = 16$) respectively (Fig. 11b). The difference between granites II and granites I is that the former are more enriched in HREE ($Gd_N/Yb_N = 2$–3) and show less fractionate trends ($La_N/Yb_N = 8$–17); like for trace elements distribution patterns these granites II and hornblende-biotite gneisses display quite similar REE patterns (Fig. 11c). Negative Eu anomalies are not significant in quartz-monzonites whereas they are more consistent in granites I (Eu/Eu* = 0.49–0.55) and pronounced in granites II (Eu/Eu* = 0.13–0.19), granitic dikes (Eu/Eu* = 0.13–0.19), and leucogranites (Eu/Eu* = 0.22–0.27). The chondrite-normalized REE pattern for the plagioclase-rich gneiss sample S4.1j is quite flat (Fig. 11c) showing no fractionation.

4.5. Geothermometry

In the ternary Qtz-Ab-Or normative diagram (Fig. 12a), the majority of biotite-granite I, granitic dikes and leucogranites compositions plot close to the granitic minimum determined experimentally at $P_{H_2O} = 2$ kb and water-undersaturated ($a_{H_2O} = 0.5$) by Holtz *et al.* (1992). The relatively high normative Or content of the natural granites may be explained by pronounced H_2O-undersaturated conditions in the source materials of these granites as for the examples observed for Harney Peak granites

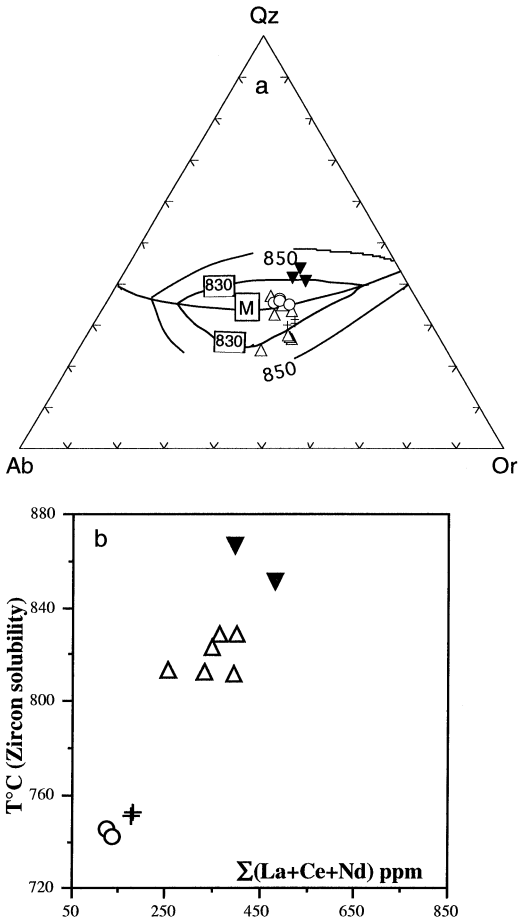

Fig. 12. a) Compositions of the Bantoum granitoids plotted in the ternary Qtz-Ab-Or normative diagram determined experimentally by Holtz et al., (1992) (at $P_{H_2O}=2$ Kb and $X_{H_2O}=0.7$). M, eutectic minimum; 830, 850, liquidus temperatures (°C).
b) Σ(La+Ce+Nd) plotted against the T°C estimated from the Zircon thermometry (Watson and Harrison, 1983) for the Bantoum granitoids. Symbols as in Fig. 5.

(Nabelek *et al*., 1992) and Gangotri leucogranites (Scaillet *et al*., 1990). Although the pressure of formation of these granites is not known, the high Or content, and therefore the generation under water-undersaturated conditions give constrains on the temperature of the melting reactions. Assuming a water activity of approximately 0.5, the minimum melt temperature is 775°C at 2 kb. This temperature would be slightly lower at higher pressure. However, the high Or content suggests that the melts leading to the crystallization of all granitic samples were formed at relatively high temperatures.

Many granitic magmas are saturated for numerous minor phases in certain trace elements, making possible their utilization as possible geothermometers in some determined circumstances. Saturation temperatures have been experimentally calibrated for zircon as a function of Zr content in granitic magma by Harrison and Watson (1983)

and Watson and Harrison (1983). The method supposes at first approximation that granitic magmas are close in composition to minimum liquid, and that the crystals of zircon are really magmatic (not inherited and free of any inherited core). Calculated temperature is that of the first appearance of zircon in the magma, and it could indicate either the temperature at which the melt was extracted from its source (Miller *et al*., 1988), or the temperatures marking the different stages of differentiation in case of fractional crystallization (*e.g* Scaillet *et al*., 1990). Hence, the more felsic granites are good candidates for calculating zircon saturation temperatures because these are commonly near minimum-temperature melts from which zircon was removed either as precipitated crystals or by fractionation of restite after partial melting. We applied that thermometer to Bantoum granitoids to get an idea about the minimum temperature of the melts (assuming that there is no residual zircon inherited from the source). Temperature ranges obtained are: 846–866℃ (biotite-granites II), 812–839℃ (biotite-granites I), 751–779℃ (granitic dikes) 719–745℃ (leucogranite) (Table 1). This thermometer can not be applied to the quartz-monzonites because these high Mg- and Ca-rocks were probably not derived from melting of crustal protoliths and the melts were not saturated with respect to zircon. Leucogranites have lower temperatures, which are consistent with those of crustal peraluminous granites; but biotite-granites have high temperature that are rather common in A-type granites (King *et al.,* 2001). Chappell *et al*. (1998) subdivided I-type granite in two groups of low- and high-temperature granites. They assumed that high-temperature I-type granitoids are characterized by chemical evolutions testifying their origin from a mafic source followed by fractional crystallization; instead, those of low temperature show evidence of chemical evolutions testifying they are originated from a partial melting of quartzo-feldspathic material followed by restite separation.

Figure 12b is the plot of the sum of LREE (La, Ce, Nd) against temperature calculated using zircon solubility method. It shows a good positive correlation and a discrimination between different granitic groups. It also suggests that concentration of Zr and LREE in these rocks may be controlled by the crystallization of zircon and other accessories phases (allanite, monazite) that used to concentrate LREE. This result is consistent with observations previously made by Broska *et al*. (2000) or Scaillet *et al*. (1990).

4.6. Sr-Nd isotopes results

Whole-rock Nd and Sr isotopic analyses were carried out on 18 samples of various petrographic groups from the Bantoum area, including quartz-monzonites, biotite-granites I, granitic dike and leucogranite. Results are listed in Table 2. Sm-Nd bulk-rock system in all of the cases couldn't define a meaningful isochron age because of narrow variation range in Sm/Nd ratios (Table 2).

Four samples of quartz-monzonites show an Rb-Sr whole-rock isochron age of 742 $\pm$61 Ma, with an initial Sr isotopic ratio of 0.70681$\pm$0.00051 and a MSWD of 0.22 (Fig. 13). Their model ages calculated relative to depleted mantle (T_{DM}) range from 1.9 Ga to 2.1 Ga.

The biotite-granites I display T_{DM} ranging from 2.1 to 2.3 Ga for most of samples (sample S4.5b gives a T_{DM}=2.7 Ga) and biotite-granites II sample S3.3b has a T_{DM}=1.7 Ga.

Table 2. Rb-Sr and Sm-Nd isotopic analytical data for gneisses and granitoids from the Bantoum area. Number in parenthesis is the 2σ error in the two last digits of the atomic ratio.

	Nd (ppm)	Sm (ppm)	$^{143}Nd/^{144}Nd$	$^{147}Sm/^{144}Nd$	$^{143}Nd/^{144}Nd$ (620 Ma)	ε_{Nd} (620 Ma)	T_{DM} (Ga)	Rb (ppm)	Sr (ppm)	$^{87}Sr/^{86}Sr$	$^{87}Rb/^{86}Sr$	$^{87}Sr/^{86}Sr$ (620 Ma)	ε_{Sr} (620 Ma)
Biotite-granite I													
S4.5b	104	19.3	0.511331(13)	0.1120	0.510876	-18.8	2.7	224	266	0.735405(11)	2.45	0.71378	142
S4.3	122	16.9	0.511302(12)	0.0839	0.510961	-17.2	2.2	231	205	0.742631(12)	3.28	0.71360	140
S2.5	81.8	11.7	0.511389(13)	0.0868	0.511036	-15.7	2.1	199	182	0.740011(12)	3.17	0.71195	116
S2.3	129	21.2	0.511438(13)	0.0995	0.511034	-15.7	2.3	211	175	0.742167(13)	3.50	0.71124	106
B00	49.3	8.88	0.511695(14)	0.1090	0.511252	-11.5	2.1	305	121	-	-	-	-
B24	60.16	8.81	0.511414(12)	0.0887	0.511054	-15.3	2.1	217	200	0.739163(11)	3.14	0.71139	108
Biotite-granite II													
S3.3b	123	21.2	0.511902(12)	0.1038	0.511480	-7.00	1.7	153	27.8	-	-	-	-
Granitic dike													
S1.4	47.1	10.3	0.511700(13)	0.1320	0.511163	-13.2	2.7	257	97.3	0.788235(12)	7.71	0.72005	231
Leucogranite													
B15	33.4	7.68	0.511741(12)	0.1390	0.511176	-13.0	2.9	370	45.5	0.928388(12)	24.0	0.71584	171
Quartz-monzonite													
B47	94.1	15.0	0.511663(13)	0.0962	0.511272	-11.1	1.9	171	1065	0.711757(14)	0.466	0.70764	55
S4.7	98.8	15.7	0.511664(11)	0.0959	0.511274	-11.0	1.9	171	1042	0.711821(14)	0.476	0.70761	55
S3.7c	79.4	12.1	0.511530(13)	0.0919	0.511157	-13.3	2.0	163	609	0.715224(12)	0.776	0.70836	65
S3.6	67.0	10.8	0.511565(11)	0.0977	0.511168	-13.1	2.1	192	615	0.716180(14)	0.904	0.70819	63
Hornblende-biotite gneiss													
S3.11	139	30.1	0.511943(12)	0.1304	0.511413	-8.32	2.2	139	57.7	0.852550(13)	7.09	0.78988	1224
S3.12	143	33.3	0.511953(14)	0.1403	0.511383	-8.90	2.5	158	39.5	0.937834(19)	11.8	0.83311	1838
B25	99	20.4	0.511802(13)	0.1244	0.511296	-10.6	2.3	205	91.8	0.858368(24)	6.55	0.80048	1374
B31	-	-	-	-	-	-	-	145	90.1	0.804744(13)	4.70	0.76314	844
Plagioclase-rich gneiss													
B43	43.8	10.1	0.512278(12)	0.1393	0.511712	-2.48	1.8	74.0	306	0.716931(09)	0.699	0.71075	99

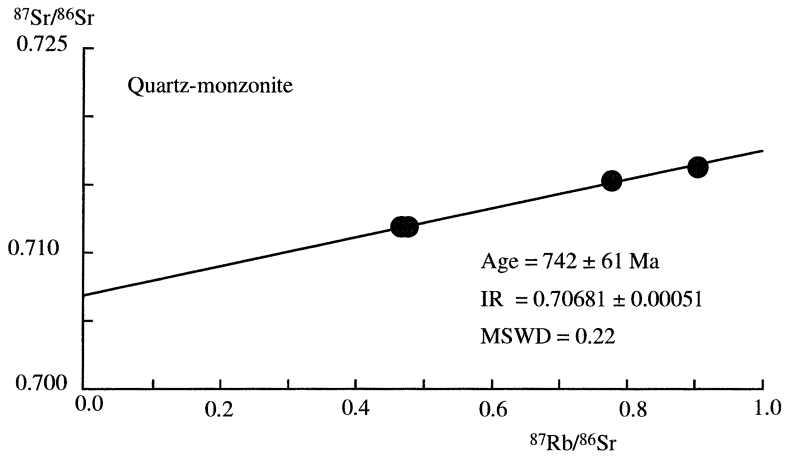

Fig. 13. Rb-Sr isochron diagram for the Bantoum quartz-monzonites.

For the granitic dike sample S1.4 $T_{DM}=2.7$ Ga. The leucogranite sample B15 shows an oldest T_{DM} of 2.9 Ga. In the Gneisses, T_{DM} range from 2.5 Ga–2.2 Ga to 1.8 Ga (plagioclase-rich gneiss B43).

5. Discussion and conclusion

The Rb-Sr whole-rock isochron age obtained for the quartz-monzonites is older than different Rb-Sr ages ranging from (575 to 657 Ma) obtained on other plutonic complexes in west Cameroon (Kwékam, 1993; Talla, 1995; Tagné Kamga, 1994); the neighboring formations of the Bangangte syenitic complex are dated at 603–606 Ma (Rb-Sr whole rock isochron; Tchouankoué, 1992), and a metadiorite at Bangoua (30 km west of Bantoum) is dated 628 Ma (U-Pb zircon; Toteu *et al.*, 2001). These ages are interpreted to be intrusion or crystallization ages.

In order to test a possibly mixing in the source materials of granitoids, we used the model initial $^{87}Sr/^{86}Sr$ ratios *vs* 1/Sr variation diagrams. For the ages above 680 Ma, plots of quartz-monzonites are scattered and biotite-granites show a meaningless strong negative correlation; and moreover, leucogranite gives an unrealistic initial $^{87}Sr/^{86}Sr$ ratio that is lower than 0.696; then an age above 680 Ma couldn't be applied the leucogranites. For 620 Ma (Fig. 14), quartz-monzonites show a positive correlation that could be interpreted as a mixing trend. We then assume that the 742 Ma isochron age to be rather a mixing line. The ongoing Rb-Sr and Sm-Nd mineral ages being carried out on selected samples from study area will help us ascertaining that issue. Calculated age for 5 samples of biotite-granites gives 543 ± 173 Ma but with poor precision due to narrow range in variation of $^{87}Rb/^{86}Sr$, and $^{87}Sr/^{86}Sr=0.71588\pm 0.00753$. Despite of this large uncertainty, this result is within the range of ages of Pan-African intrusives in CAFB, and it confirms at least that biotite-granites are younger than quartz-monzonites as it is suggested by field relationships (*e.g.* no enclave observed in quartz-monzonites, but both enclaves of quartz-monzonites and gneisses are found in biotite-granites).

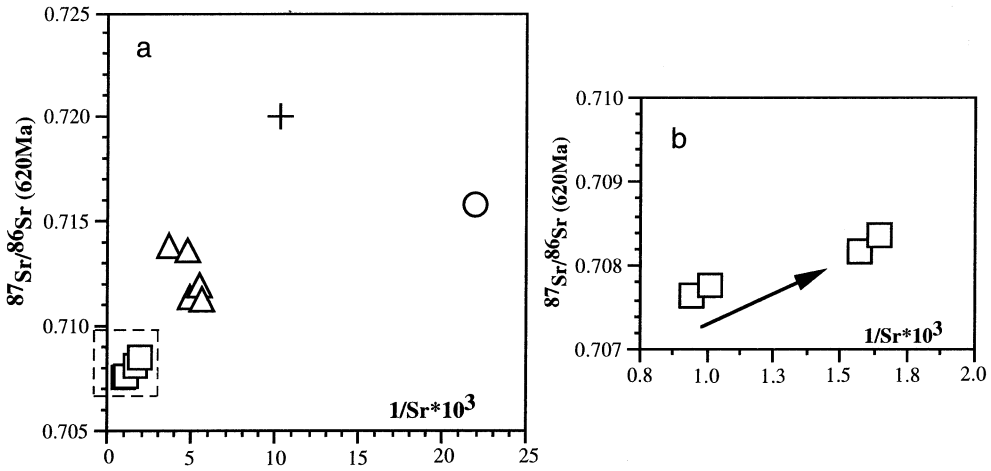

Fig. 14. a) $^{87}Sr/^{86}Sr$ (620 Ma) vs 1/Sr variation diagram for the granitoids. b) Enlargement of the squared area in a) for quartz-monzonites; the arrow shows the possibly mixing trend. Symbols as in Fig. 5.

Extrapolations to T_{DM} for plutonic rocks can have large uncertainties due to possible REE fractionation during magma genesis if they are much younger than their source terranes, as is the case for *ca* 500–650 Ma Pan-African granitoids intruding and presumably derived from Archean to Paleoproterozoic basement in parts of the CAFB. As a result, we have chosen 620 Ma as the main reference time for Nd compositions in the past as well as Sr and Nd initial ratios, since we can extrapolate accurately to that time without worrying about possible fractionation of Sm-Nd during either magma genesis or high-grade metamorphism; and furthermore it corresponds to the average age of most of plutons in CAFB.

For quartz-monzonites, initial $^{87}Sr/^{86}Sr$ ratios (SrI) calculated using 620 Ma vary from 0.70761 to 0.70836; their ε_{Nd} (620 Ma) range from −13.3 to −11.0.

The biotite-granites I display model SrI (620 Ma) ranging from 0.71124 to 0.71378. They have model initial $^{143}Nd/^{144}Nd$ ratios of 0.51130–0.51170 and ε_{Nd} (620 Ma) from −18.8 to −11.5.

The granitic dike sample S1.4 gives a high initial Sr isotopic ratio (620 Ma) = 0.72005. It's model initial $^{143}Nd/^{144}Nd$ ratio = 0.51116 and the ε_{Nd} (620 Ma) is −13.2.

The leucogranite sample B15 has a SrI (620 Ma) = 0.71584. It's model initial $^{143}Nd/^{144}Nd$ ratio = 0.51118 and the ε_{Nd} (620 Ma) is −13.0.

Gneisses have higher model SrI, whose values show a larger spread. These model SrI (620 Ma) are 0.71075 (B43, Pl-rich gneiss), 0.76314 (B31, Grt-gneiss) and 0.78988–0.83311 (Hb-Bt gneiss). Model initial $^{143}Nd/^{144}Nd$ ratios are 0.51138–0.51171, with ε_{Nd} (620 Ma) ranging from −10.6~−8.3 to −2.5 for the plagioclase-rich gneiss sample B43.

The variation in the values of the initial $^{87}Sr/^{86}Sr$ ratios in the different groups of granitoids is indicative of the heterogeneity in their source rocks. These $^{87}Sr/^{86}Sr$ initial ratios are high suggesting parental magmas were, therefore, derived from, or contaminated with different crustal sources with relatively high concentration of radiogenic

^{87}Sr; the lowest values observed in quartz-monzonites show that they have more deep-seated origin.

Overall, T_{DM} ages of investigated samples range from 1.8 to 2.9 Ga with most of them being grouped around 2.1–2.3 Ga, and they have large negative values of ε_{Nd} (620 Ma) from −19 to −13. The large negative initial ε_{Nd} values of the granitic rocks is evocative of their long and complex crustal history. These Nd isotopic signatures confirm the presence of remnants of a lower Paleoproterozoic or Archean crust in that domain of the CAFB (Penaye *et al*., 1993; Toteu *et al*., 1994a, 2001). Relatively lower values of initial Sr and Nd ratios observed in quartz-monzonites point to an involvement of a significant amount of juvenile magma. This result is in agreement with observations by Toteu *et al*. (2001) that Pan-African granitoids southeast of the Banyo-Tcholliré shear zone (Fig. 1) are generated mainly by melting of older (Eburnean) crust with limited inputs of juvenile magmas. Sr-Nd isotopic characteristics of gneisses are significantly different from those of associated granitoids as illustrated in Fig. 15a, showing that they may have different history and no genetic link. For the plagioclase-rich gneiss sample B43, higher ε_{Nd} value (−2.5) and lowest T_{DM} age suggests it may contain volcanic material in its protolith. The field of compositions of some Archean syenites and high-K granitoids from the Ntem complex is shown on Fig. 15b. The Bantoum granitoids plot in the continuation of the field of these Archean rocks, suggesting that source materials similar to these high-K granitoids and syenites from the Archean Ntem complex (Tchameni *et al*., 2000, 2001) could be good candidate for the protoliths of the Bantoum granitoids. On the ε_{Nd} *vs* time diagram (Fig. 16), the evolution of ε_{Nd} values of Bantoum granitoids emphasizes that they can be formed by partial melting of old material with an isotope signatures similar to those of Archean crust from of the Ntem complex during the Pan-African orogenesis. However, combined zircon U-Pb ages and Sm-Nd data in other parts of CAFB in Cameroon have led

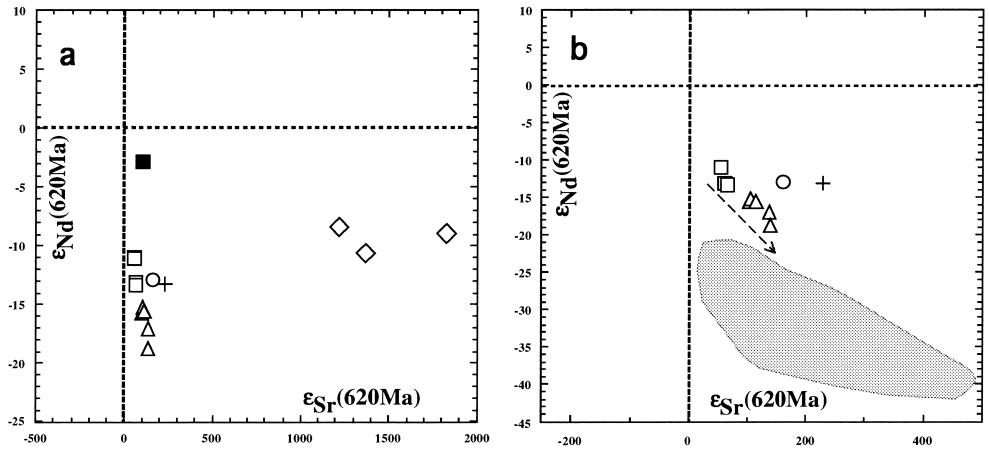

Fig. 15. a) Model initial ε_{Nd} vs ε_{Sr} diagram for granitoids and gneisses; b) Model initial ε_{Nd} vs ε_{Sr} diagram for the Bantoum granitoids. Shaded area corresponds to compositions of Archean syenites and high-K granitoids from the Congo craton (data from Tchameni et al., 2000; 2001). Symbols as in Fig. 5.

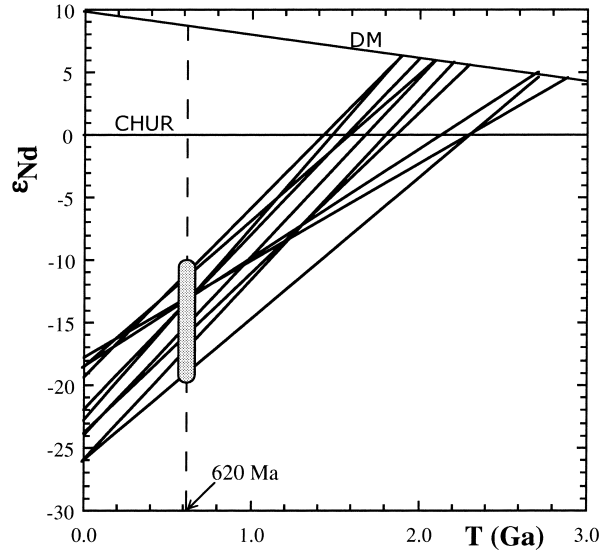

Fig. 16. ε_{Nd} *vs time variation diagram for granitoids, showing the significant contribution of a Paleoproterozoic to Archean crust in their protolith.*

Toteu *et al*. (1994a, 2001) to conclude that the Archean crust was not directly involved as the source for protoliths of Pan-African granitoids as it was completely recycled during the 2100 Ma (Eburnean) event.

The overall geochemical features of investigated rocks are compatible with compositions of calc-alkaline magmas in orogenic domains and are similar to those documented in numerous huge Pan-African plutons in west Cameroon (*e.g.* Nguiessi Tchankam *et al*., 1997); particularly their hyperpotassic calc-alkaline trends are characteristic of a continental collision framework (Black and Liegeois, 1993; Liegeois *et al*., 1994). Therefore within-plate granite (WPG) trace element character of granites II and gneisses (Fig. 10) is probably not indicative of the tectonic framework during their formation, and could be interpreted as being inherited from the source of their protolith. Liegeois *et al*. (1994) attributed such trace element character of granitoids from the Tuareg Shield to crustal delamination operating in a syn- to post-collisional geodynamic setting.

Our data also suggest that the difference in geochemical nature between the different groups of granitoids in the study area is not necessarily related to changes in tectonic framework but is more probably due to variations in the mechanisms of magma production in the crust. Besides the source material, water contents and melting temperatures for example are known to be critical variables as evidenced by investigations of Clemens and Vielzeuf (1987) and Johannes and Holtz (1990). Low water activities or melting due to fluid-absent dehydration reactions explain partial melting at higher temperatures for the formation of the granites. In such a case, there is more efficient dissolution of residual mineral phases such as zircon, apatite, monazite and sphene in the melts, and as a result, an increase in the HFSE and REE contents in the

produced melts. Examples of plutonism in which, depletion in water of the crustal source have imposed changes in the melting conditions during subsequent events of production of granite magmas, have been documented by Whalen *et al*. (1987) and Pimentel *et al*. (1996). In most of the cases, it is likely that the input of heat required to promote large-scale melting of the crust was most probably provided by the introduction of mafic magmas into the crust (Roberts and Clemens, 1993).

Neither geochemical features nor isotopic data of the Bantoum area granitoids supports the eventuality of a formation of biotite-granites by differentiation processes from quartz-monzonites. On the basis of these chemical and isotopic characteristics, it appears that the investigated rocks in the Bantoum area could be subdivided at least into four groups: quartz-monzonites, biotite-granites, leucogranites and gneisses. Each group among granitoids crystallized at different temperatures and from different source materials during the same orogenic event; but there is an important participation of the older Eburnean material in their protoliths. Among biotite-granites, a few part (biotite-granites II) share the same geochemical features as the hornblende-biotite gneisses, notably similar chondrite-normalized trace elements and REE distribution patterns and their position in the same field in tectonic discrimination diagrams, suggesting the contribution of these gneisses to the protolith of some biotite-granites. Results of melting and crystallization experiments carried out on an amphibole-biotite gneiss (Nzolang *et al*., in prep.) show that compositions of experimental liquids produced from that gneiss are comparable solely to those of granites II, supporting that amphibole-biotite gneiss is a possible source for biotite-granites II.

Acknowledgments

The first author is grateful to the German Academic Exchange Service (DAAD) for providing fellowship support for a research stay in Germany and Institut of Mineralogy of University of Hannover for its hospitality, and the Japanese Ministry of Education, Science, Culture and Sports (Monbusho) for the ongoing scholarship. H. Ishimoto, J. Ishioka, N. Nishi and S. Suzuki (Niigata University) are thanked for assistance during XRF and isotope analyses. The comments of two anonymous reviewers are greatly appreciated. A part of this work was supported by a Grant-in-Aid for Scientific Research of the Ministry of Education, Japan (No. 13373005, Prof. M. Arima; Yokohama National University).

References

Ayuso, R. and Arth, J.G. (1992): The Northeast Kingdom batholith, Vermon: magmatic evolution and geochemical constraints on the origin of Acadian granitic rocks. Contrib. Mineral. Petrol., **111**, 1–23.

Berthé, D., Choukroune, P. and Jegouzo, P. (1979): Orthogneiss, mylonite and non coaxial deformation of granite: The example of the South Armorican Shear Zone. J. Struct. Geol., **1**, 31–42.

Bertrand, J.M., Dupuy, C., Dostal, J. and Davidson, I. (1984): Geochemistry and geotectonic interpretation of granitoids from Central Iforas (Mali, West Africa). Precambrian Res., **26**, 265–283.

Bessoles, B. and Trompette, M. (1980): Géologie de l'Afrique: la chaîne panafricaine, "zone mobile d'Afrique Centrale (partie sud) et zone mobile soudanaise". Mém. BRGM, Orléans, France, **92**, 378 p.

Black, R. and Liegeois, J.P. (1993): Cratons, mobile belts, alckaline rocks and continental lithospheric mantle:

the panafrican testimony. J. Geol. Soc. London, **150**, 89–98.
Broska, I., Petrík, I. and Williams, C.T. (2000): Coexisting monazite and allanite in peraluminous granitoids of the Tribec Mountains, Western Carpathians. Am. Mineral., **85**, 22–32.
Chappell, B.W. and White, A.J.R. (1992): I- and S-type granites in the Lachlan Fold Belt. Trans. R. Soc. Edinburg, **83**, 1–12.
Chappell, B.W., Bryant, C.J., Wyborn, D., White, A.J.R. and Williams, I.S. (1998): High- and low-temperature I-type granites. Resource Geol., **48**, 225–235.
Clemens, J.D. and Vielzeuf, D. (1987): Constrains on melting and magma production in the crust. Earth Planet. Sci. Lett., **86**, 287–306.
Debon, F. and Le Fort, P. (1983): A chemical-mineralogical classification of common plutonic rocks and associations. Trans. R. Soc. Edinburgh, **73**, 135–149.
Déruelle, B., Moreau, C., Nkoumbou, C., Kambou, R., Lissom, J., Njongfang, E., Ghogomu, R.T. and Nono, A. (1991): The Cameroon Line: a review. Magmatism in Extensional Structure Settings, The Phanerozoic African Plate, ed. by A.B. Kampuzu and T. Lubala. Berlin, Springer, 274–327.
Goldstein, S.L., O'Nions, R.K. and Hamilton, P.J. (1984): A Sm-Nd study of atmospheric dusts and particulates from major river systems. Earth Planet. Sci. Lett., **70**, 221–236.
Harris, N.B.W., Pearce, J.A. and Tindle, A.G. (1986): Geochemical characteristics of collision-zone magmatism. Collision Tectonics, ed. by M.P. Coward and A.C. Ries. Blackwell, Geol. Soc., 67–81 (Geol. Soc. Spec. Publ., 19).
Harrison, T.M. and Watson, E.B. (1983): Kinetics of zircon dissolution and zirconium diffusion in granitic melts of variable water contents. Contrib. Mineral. Petrol., **84**, 66–72.
Holtz, F., Pichavant, M., Barbey, P. and Johannes, W. (1992): Effects of H_2O liquidus phase relations in the haplogranitic system at 2 and 5 kbar. Am. Mineral., **77**, 1223–1241.
Johannes, W. and Holtz, F. (1990): Formation and composition of H_2O-undersaturated granitic melts. High Temperature Metamorphism and Crustal Anatexis, ed. by J.R. Asworth and M. Brown. London, Unwin Hyman, 87–105.
Kagami, H., Iwata, M., Sano, S. and Honma, H. (1987): Sr and Nd isotopic compositions and Rb, Sr, Sm and Nd concentrations of standard samples. Tech. Rep. ISEI Okayama Univ., **B4**, 1–16.
Kawano, Y. (1994): Calculation program for isochron ages of Rb-Sr and Sm-Nd systems using personal computer. Geoinformatics, **5**, 13–19 (in Japanese with English abstract).
King, P.L., Chappell, B.W., Allen, M. and. White, A.J.R. (2001): Are A-type granites the high-temperature felsic granites? Evidence from fractionated granites of the Wangrah Suite. Aust. J. Earth Sci., **48**, 501–514.
Kretz, R. (1983): Symbols for rock-forming minerals. Am. Mineral., **68**, 277–279.
Kwékam, M. (1993): Le massif plutonique calco-alcalin pan-africain de Fomopéa (Ouest-Cameroun). Cadre structural-Pétrologie-Géochimie, Interprétation géodynamique. Thèse Doctorat 3eème cycle, Univ. Yaoundé I, Cameroon, 154 p.
Lameyre, J. (1973): Les marques de l'eau dans les leucogranites du Massif Central français. Bull. Soc. Geol. France, **7**, XV, 288–295.
Lasserre, M. (1966): Géochronologie du Cameroun. Rapport d'activité scientifique (1962 à 1966). Measures d'âges absolus sur micas et sur roches totales. Technique et discussion des resultats. B.R.G.M., Paris-orléans, 74 p.
Lasserre, M. (1967): Données géochronologiques nouvelles acquises au 1er Janvier 1967 par la méthode au strontium appliquée aux roches cristallophylliennes du Cameroun. Ann. Fac. Sci. Univ. Clermond Ferrand, **36**, 109–144.
Liegeois, J.P., Black R., Navez J. and Latouche L. (1994): Early and late Pan-African orogenies in the Aïr assembly of terranes (Tuareg Shield, Niger). Precambrian Res., **67**, 59–88.
Lugmair, G.W. and Marti, K. (1978): Lunar initial $^{143}Nd/^{144}Nd$: differential evolution of the Lunar crust and mantle. Earth Planet. Sci. Lett., **39**, 349–357.
Miller, C.F., Watson, E.B. and Harrison, T.M. (1988): Perspectives on source, segregation and transport of granitoid magma. Trans. R. Soc. Edinburg, Earth Sci., **79**, 129–133.
Nabelek, P.I., Russ-Nabelek, C. and Denison, J.R., (1992): The generation and crystallization conditions of the Proterozoic Harney Peak leucogranite, Black Hills, South Dakota, USA: petrologic and

geochemical constraints. Contrib. Mineral. Petrol., **110**, 173–191.

Nakamura, N. (1974): Determination of REE, Ba, Fe, Mg, Na and K in carbonaceous and ordinary chondrites. Geochim. Cosmochim. Acta, **38**, 757–775.

Ngako, V., Jegouzo, P. and Nzenti, J.P. (1991): Le Cisaillement Centre Camerounais. Rôle structural et géodynamique dans l'orogenèse panafricaine. C.R. Acad. Sci., Paris, **313**, 457–463.

Ngako, V., Jegouzo, P. and Nzenti, J.P. (1992): Champ de raccourcissement et cratonisation du Nord-Cameroun du Protérozoïque supérieur au Paléozoïque moyen. C.R. Acad. Sci., Paris, **315**, 371–377.

Ngnotué, T., Nzenti, J.P., Barbey, P. and Tchoua, F.M. (2000): The Ntui-Bétamba high-grade gneisses: a northward extension of the Pan-African Yaoundé gneisses in Cameroon. J. Afr. Earth Sci., **31**, 369–381.

Nguiessi Tchankam, C. and Vialette, Y. (1994): Données géochronologiques (Rb-Sr, Pb-Pb, U-Pb) sur le complexe plutonique de Bandja (centre-ouest Cameroun). C.R. Acad. Sci., **319**, 317–324.

Nguiessi Tchankam, C., Nzenti, J.P., Nsifa, E.N., Tempier, P. and Tchoua, F.M. (1997): Les granitoïdes calco-alcalins, syncisaillement de Bandja dans la chaîne panafricaine nord-équatoriale au Cameroun. C.R. Acad. Sci., **325**, 95–101.

Nzenti, J.P. (1987): Pétrogenèse des migmatites de Yaoundé (Cameroun), éléments pour un modèle géodynamique de la chaîne Pan-Africaine Nord-Equatoriale. Thèse, Univ. Nancy I., France, 147 p.

Nzenti, J.P., Barbey, P., Macaudière, J. and Soba, D. (1988); Origin and evolution of the late Precambrian high-grade Yaoundé gneisses (Cameroon). Precambrian Res., **38**, 91–109.

Nzenti, J.P., Ngako, V., Kambou, R., Penaye, J., Bassahak, J. and Njel O.U. (1992): Structures régionales de la chaîne panafricaine du Nord-Cameroun. C.R. Acad. Sci., Paris, **315**, 209–215.

Pearce, J.A., Harris, N.B.W. and Tindle, A.G. (1984); Trace elements discrimination diagrams for the tectonic interpretation of granitic rocks. J. Petrol., **25**, 956–983.

Penaye, J., Toteu, S.F., Michard, A., Bertrand, J.M. and Dautel, D. (1989) Reliques granulitiques d'âge Protérozoïque inférieur dans la zone mobile Panafricaine d'Afrique Centrale au Cameroun; Géochronologie U-Pb sur zircons. C.R. Acad. Sci. Paris, **309**, 315–318.

Penaye, J., Toteu, S.F., Van Schmus, W.R. and Nzenti, J.P. (1993): U-Pb and Sm-Nd preliminary data on the Yaoundé series, Cameroon: re-interpretation of the granulitic rocks as the suture of a collision in the 'Centrafrican belt'. C.R. Acad. Sci. Paris, **317**, 789–794.

Pimentel, M.M., Fuck, R.A. and Alvarenga, C.J.S. (1996): Post-Brasiliano (Pan-African) high-K granitic magmatism in central Brazil: the role of Late Precambrian-early Paleozoic extension. Precambrian Res., **80**, 217–238.

Roberts, M.P. and Clemens, J.D. (1993): Origin of high-potassium, calc-alkaline, I-type granitoids. Geology, **21**, 825–828.

Scaillet, B., France-Lannord, C. and Le Fort, P. (1990): Badrinath-Gangotri plutons (Garhwal, India): petrological and geochemical evidence for fractionation processes in a high Himalayan leucogranite. J. Volcanol. Geotherm. Res., **44**, 163–188.

Soba, D. (1989): La série du Lom: étude géologique et géochronologique d'un bassin volcano-sédimentaire de la chaîne panafricaine à l'est du Cameroun. Thèse Doct. Etat, Univ. Paris VI, France, 181 p.

Steiger, R.H. and Jäger, E. (1977): Subcommission on geochronology: convention on the use of decay constants in geo- and cosmo-chronology. Earth Planet. Sci. Lett., **36**, 359–362.

Tagné Kamga, G. (1994): Le complexe plutonique panafricain de Ngondo (Ouest Cameroun): Structure et pétrogenèse. Thèse, Univ. Franche-Comté, France, 236 p.

Tagné Kamga, G., Mercier, E., Rossy, M. and Nsifa, E.N. (1999): Synkinematic emplacement of the panafrican Ngondo igneous complex (west Cameroon, central Africa). J. Afr. Earth Sci., **28**, 675–691.

Talla, V. (1995): Le massif granitique panafricain de Batié (Ouest Cameroun): Pétrologie-Pétrostructurale-Gèochimie. Thèse Doctorat 3ème cycle, Univ. Yaoundé I, Cameroon, 144 p.

Tanaka, T., Togashi, S., Kamioka, H., Amakawa, H., Kagami, H., Hamamoto, T., Yuhara, M., Orihashi, Y., Yoneda, S., Shimizu, H., Kunimaru, T., Takahashi, K., Yanagi, T., Nakano, T., Fujimaki, H., Shinjo, R., Asahara, Y., Tanimizu, M. and Dragusanu, C. (2000): JNdi-1: a neodymium isotopic reference in consistency with LaJolla neodymium. Chem. Geol., **168**, 279–281.

Tchameni, R., Mezger, K., Nsifa, E.N. and Pouclet, A. (2000) Late Archean crustal evolution in the Congo

Craton: evidence from the K-rich granitoids of the Ntem Complex, Southern Cameroon. J. Afr. Earth Sci., **30**, 133–147.

Tchameni, R., Mezger, K., Nsifa, E.N. and Pouclet, A. (2001): Crustal origin of Early Proterozoic syenites in the Congo Craton (Ntem Complex, South Cameroon). Lithos, **57**, 23–42.

Tchouankoué, J.P. (1992): La Syénite de Bangangté: Un complexe pan-africain à caractères intermediaires. Pétrologie-Géochimie. Thèse Doctorat 3ème Cycle, Univ. Yaoundé, Cameroon, 130 p.

Thompson R.N., Morrison M.A., Hendry G.L. and Parry S.J. (1984): An assessment of the relative roles of crust and mantle in the magma genesis: an elemental approach. Phil. Trans. R. Soc. London, **A310**, 549–590.

Toteu, S.F., Michard, A., Bertrand, J.M. and Rocci, G. (1987): U: Pb dating of Precambrian rocks from northern Cameroon, orogenic evolution and chronology of the Pan-African belt of central Africa. Precambrian Res., **37**, 71–87.

Toteu, S.F., Penaye, J., Van Schmus, W.R. and Michard, A. (1994a): Preliminary U-Pb and Sm-Nd geochronologic data on the north-central Cameroon: contribution of an Archean and Paleoproterozoic crust to the edification of an active domain of the Pan-African orogeny. C.R. Acad. Sci, Paris, **319**, 1519–1524.

Toteu, S.F., Van Schmus, W.R., Penaye, J. and Nyobe, J.B. (1994b): U-Pb and Sm-Nd evidence for Eburnean and Pan-African high-grade metamorphism in cratonic rocks of southern Cameroon. Precambrian Res., **67**, 321–347.

Toteu, S.F., Van Schmus, W.R., Penaye, J. and Michard, A. (2001): New U-Pb and Sm-Nd data from north-central Cameroon and its bearing on the pre-Pan African history of central Africa. Precambrian Res., **108**, 45–73.

Villa, I.M., Ruggieri, G. and Puxeddu, M. (1997): Petrological and geochronological discrimination of two white-mica generations in a granite cored from the Laderello-Travale geothermal field (Italy). Eur. J. Mineral., **9**, 563–568.

Watson, E.B. and Harrison T.M. (1983): Zircon saturation revisited: temperature and composition effects in a variety of crustal magma types. Earth Planet. Sci. Lett., **64**, 295–304.

Weecksteen, G. (1957): Notice explicative sur la feuille Douala-Est avec carte géologique de reconnaissance au 1/500.000. Dir. Min. Geol., Yaoundé, Cameroun, 39 p.

Whalen, J.B., Currie, K.L. and Chappell, B.W. (1987): A-type granites: geochemical characteristics, discrimination and petrogenesis. Contrib. Mineral. Petrol., **95**, 407–419.

York, D. (1966): Least-squares fitting of a straight line. Can. J. Phys., **44**, 1079–1086.